Interner Bericht
DESY S1-73/7
September 1973

Proton Acceleration in DESY

by

W. Ebeling, A. Febel, B. Hellwig, G. Hemmie, G. Jacobs
H. Kumpfert, M. Nagl, F. Pieper

Hamburg, Sept. 73

PROTON ACCELERATION IN DESY

1. Introduction

Following preliminary studies [1], [2], [3] the purpose of this paper is to collect the necessary data for proton generation and acceleration in DESY.

2. The Preaccelerator

For reasons of economy a proton linac was no longer considered after it turned out that a commercially available standard electrostatic accelerator ("Van de Graaff") would just be good enough to do the job. An order was placed with Electrostatic International, Inc. (NEC), Middleton, Wisconsin, USA.

2.1 The proton beam data

Kinetic Energy	T	4.0	MeV
Momentum	p	86,73	MeV/c
Voltage Stability	ΔV	$\pm$ 2	kV
Beam Phase Space at T = 4 MeV	$\varepsilon = \frac{F}{\pi}$	$6 \cdot 10^{-6}$	rad·m
Pulsed Peak Proton Current, Design Aim	i	20	mA
Pulsed Peak Proton Current, Acceptance Test	i	10	mA
Pulse Repetition Rate		max. 1	sec^{-1}
Pulse Length, variable	τ	15 - 60	μsec
Energy Change during Pulse	ΔT	max. 1.0	keV
Beam Size and Divergence 1 m from End of Tank for i = 10 mA	Radius	1.75	cm
	Divergence	$1.06 \cdot 10^{-3}$	rad

2.2 Machine Stabilization

The voltage of max. 4 kV due to the discharge of the terminal (i = 20 mA, τ = 60 us, C = 300pF) will be compensated by means of a voltage on a capacitor shell provided inclusive the necessary electronics by the manufacturer.

In addition to this fast (intrapulse) stabilization slow (pulse to pulse and longtime) stabilization is achieved by means of a triode corona feedback loop using an error signal e.g. from the energy analysing slits in the beam transport system between the proton source and the synchrotron.

2.3 The Ion Source

For the ion source, NEC plans to use a duoplasmatron similar to the one used at LAMPF. This source is reported to have a life time of at least 1000 hours; 75 - 80 % of the ion current consists of protons [4].

The transverse phase space acceptance of the synchrotron is larger than the emittance of the 4 MeV proton beam from the source ($\varepsilon = 6 \cdot 10^{-6}$ rad·m). Since one would like to have $30 \cdot 10^{-6}$ rad·m because of the Laslett space charge limit [3] , the emittance of the beam has to be increased before injection. Unfortunately this could not be achieved by modifying the proton source, because the small diameter of the accelerator tube does not allow the transport of wider beams [5].

2.4 Location of the Electrostatic Accelerator

The location of the Van de Graaff Generator will be the socalled "Inner Experimental Area" directly adjacent to the synchrotron tunnel (Fig. No. 1). The protons will be injected opposite to the direction of normal electron acceleration into the synchrotron.

3. Beam Transport and Injection into the Synchrotron

3.1 Optics of the Beam Transport System

Fig. 2 shows a possible solution for the optics of the proton injection beam transport system. The optics provides a waist at a location for a beam position monitor delivering an error signal for the Van de Graaff energy servo feed back loop. In the waist any change in momentum will produce a big horizontal beam displacement. Dispersion matching between magnet M 1 and the synchrotron is not necessary because of the small momentum spread of $\frac{\Delta p}{p} = 5 \cdot 10^{-4}$ bin. In fig. 2 the dispersion-curve D corresponds to $\frac{\Delta p}{p} = + 12{,}5 \cdot 10^{-4}$.

Enveloppe matching is effected by means of lenses Q 1 to Q 4. There is a choice of equivalent solutions all using the same magnet and lense positions. We assumed $\varepsilon = \frac{F}{\pi} = 30 \cdot 10^{-6}$ rad·m for both the horizontal and vertical emittance.

All magnets and lenses necessary in this beam transport-system are available as spare parts of older systems on the DESY area. Lenses Q 1, Q 2, Q 3, Q 4 are of type QL as used in the beam transport systems connecting linac II, synchrotron, and storage rings. The power supplies are partly available, the missing ones can be easily manufactured in the DESY electronic workshop.

3.2 Increase of the Beam Emittance (see chapter 2.3)

In principle it is possible to increase the emittance of a beam by multiple scattering e.g. in a gas scattering chamber between Q 2 and Q 3 (see fig. 2). The pressure in the chamber is given by

$$P\,[\mathrm{Torr}] = \frac{2.91 \cdot 760}{15} \cdot (pc)^2 \beta^2 \frac{\Delta \varepsilon}{\beta_s} \cdot \frac{1}{L}$$

with $pc = 86{,}7$ MeV

$\beta_s = 10$ m/rad

$\Delta\varepsilon = (30 - 6) \cdot \text{rad} \cdot \text{m} = 24 \cdot 10^{-6}$ rad·m

L = 0,5 m

β = 0,092

follows

P = 0,3 Torr

The scattering causes a negligible additional energy spread. The pressure of P = 0,3 Torr however, will be a problem for differential pumping, since the pressure in the synchrotron will have to be in the order of $3 \cdot 10^{-8}$ Torr. Therefore, alternative solutions as thin foils or carbon fiber grids must be considered.

3.3 Injection into the Synchrotron

Both single turn and multiturn injection will be provided. The system will consist of

1) a fast beam bump (for multiturn injection)
2) a kicker (for single turn injection)
3) a septum magnet

3.3.1 Fast Beam Bump for Multiturn Injection

For the generation of the bump, three air coils will be provided on the (proton-) down stream ends of synchrotron F-magnets 19,21, and 23 (see Fig. 3).

The injection point is defined as the end of the septum, i.e. 568 mm upstream of the steel of D-Magnet 20 (proton beam direction is taken for reference). At the injection point the beam displacement with respect to the equilibrium orbit is - 44,6 mm, the angle is 9,4 mrad. The necessary angles for the three air-coil dipole "kicks" are

at 19 : α_{19} = - 4,39 mrad

at 21 : α_{21} = - 0,63 mrad

at 23 : α_{23} = - 4,39 mrad

The injection efficiency was estimated with 55%, assuming the following numbers :

Synchrotron hor. accept. A = 100π mrad·mm,
Emittance of injected beam F = 20π mrad mm,
linear decrease of fast bump amplitude during five turns (or 57,4 μsec)

For this case the area occupied in the transverse phase space of the synchrotron turns also out to be 55%.

The coil length (in the azimutal direction) can be made 20 cm, the distance of the coil center from the F-magnet steel being 15 cm. The coils have to be air coils in order to avoid eddy currents and field distortions induced by the main synchrotron magnet stray field. Fig. 4 gives a cross sectional view of the conductor arrangement.

Since the injection efficiency is not influenced too much, the current versus time programming for the injection beam bump coils must only roughly meet the condition of linear decrease to zero during the time of 5 turns (57,4 μsec for protons with a momentum of 87 MeV/c).

So a condenser discharge type time function (Fig. 5) is sufficient which allows a simple and cheap pulser circuit. The particle transit time from magnet 19 to magnet 23 is approx. 1 μsec which is fast compared to the rate of bump amplitude decrease with time.

3.3.2 Fast Kicker for Single Turn Injection

For single turn injection the beam displacement from the equilibrium orbit will be - 56,7 mm, and the angle 11,93 mrad at the injection point. The air coil at magnet 19 has to generate a kick of 5,58 mrad the duration of which has to be short compared to the orbit time (say 1 μsec compared to 11,47 μsec). The kicker pulser (see Fig. 6) in this case will be connected directly to coil 19. Fig. 7 shows the current versus

time.

3.3.3 Injection Septum

Fig. 8 shows the geometry and the particle trajectory by which the data of the septum are determined. Fig. 9 shows the septum cross section.

Further details of the septum :

max. current strip thickness	2,5 mm
flux density	0,26 Tesla
current	8300 A
inductance	1 μH
mechanical force	5,2 kp/block

This force will be tolerable, if the copper current strip is reenforced by a stainless strip brazed to the copper strip. Outside the gap area the stainless strip will be laminated in order to avoid bypass currents.

To restrict the max. betatron oscillation amplitude induced by errors in the septum current to less than 1 mm this current has to be accurate within $\pm 3 \cdot 10^{-4}$.

Fig. 10 shows the septum current versus time. It is a sine half wave with T = 6,7 msec and a repetition rate of one puls in three seconds. The power dissipation will be less than 10 W. So no water cooling is needed.

4. Radio Frequency Acceleration

4.1 Peak Accelerating Voltage per Turn under Consideration of Space Charge

We plan for adiabatic capture. Aside from the ideal case $\dot{B}= \varphi_s=0$ this means that any change with time be slow compared to the duration of a synchrotron oscillation period.

B Magnetic flux density

φ phase angle between particle and zero crossing of RF-voltage

s index refers to the synchronous particle

4.1.1 For $\dot{B} = \dot{\varphi}_s = 0$, and using [6], p. 31 the bucket half height is

$$\Delta T = \frac{\bar{h}}{2} \cdot \Delta T_{inj} = \frac{\bar{h}}{2} \cdot T \cdot \left(\frac{\Delta T}{T} \right) = \bar{\eta} \cdot T \cdot \left(\frac{\Delta p}{p} \right)$$

where $\pm \Delta T_{inj}$ is the energy spread of the injected beam. If we use the curves of [6, p. 31] for $\varphi_s = 0$, we find

$$\alpha(\bar{\Gamma}) = 1 \; ; \quad Y(\bar{\Gamma}) = \sqrt{2}.$$

With these values and the formulae for bucket area and bucket half height as given in the table of [6, p. 31], the bucket area A_{sp} will turn out to be $A_{sp} = 8 \cdot$ (bucket half height) or :

$$A_{sp} = 8 \bar{\eta} T \left(\frac{\Delta p}{p} \right) \qquad (1)$$

The subscript sp indicates that this expression is valid in the presence of space charge.

On the other hand, the bucket area without consideration of space charge is

$$A = 16 \beta \sqrt{\frac{e \cdot V \cdot E}{2 \pi h |\eta|}} \qquad (2)$$

(see [6, p. 31]). From [6, p. 32] and [9] we take

$$\frac{A_{sp}}{A} = \sqrt{1 - g_c \cdot e \cdot h \cdot N / 4\pi\varepsilon_0 R V \gamma^2} \qquad (3)$$

where

$$g_c = 1 + \ln \left(\frac{\text{vacuum chamber diameter}}{\text{beam diameter}} \right)$$

Combining equation (2) and (3) :

$$A_{sp}^2 = \frac{16^2 \cdot \beta^2 \cdot e \cdot V \cdot E}{2 \pi h \eta} \left(1 - \frac{g_c \cdot e \cdot h \cdot N}{4 \pi \varepsilon_o \gamma^2 \cdot R \cdot V} \right)$$

From this, the peak accelerating voltage turns out to be

$$V = \frac{2 \pi h \eta}{16^2 \beta^2 e \cdot E} \cdot A_{sp}^2 + \frac{g_c \cdot e \cdot h \cdot N}{4 \pi \varepsilon_o \gamma^2 R}$$

or, using equation (1) :

$$V = \frac{\pi^3 h \eta}{2 \beta^2 E \cdot e} T^2 \left(\frac{\Delta p}{p}\right)^2 + \frac{g_c \cdot e \cdot h \cdot N}{4 \pi \varepsilon_o \gamma^2 R} \qquad (5)$$

We must keep in mind that with our definitions, equation (5) is only valid for $\gamma_s = 0$. Comparing (5) with (2) we learn that due to space charge additional voltage is required. Numbers are given in the following table :

peak accelerating voltage per turn for $\left(\frac{\Delta p}{p}\right)_i = \pm 2.5 \cdot 10^{-4}$

h	V
11	0,18 kV
22	0,36 kV
33	0,54 kV

$\frac{\Delta p}{p} = \pm 2{,}5 \cdot 10^{-4}$ momentum spread of electrostatic accelerator beam

$\frac{\text{vac. chamber dia.}}{\text{beam dia.}} \stackrel{!}{=} 2$

$N = 2.1 \cdot 10^{11}$ number of protons to be accelerated per synchrotron puls (Laslett space charge limit at injection momentum of 87 MeV/c, see [3, p. 4]).

$R = 50.4$ m average radius of synchrotron

$\beta = 0.092$

$\eta = \gamma_{tr}^{-2} - \gamma^{-2} = 0.96$ for $T_{inj} = 4$ MeV ($P_{inj} = 86.73$ MeV/c)

$E = 9.42 \cdot 10^5$ keV

$\gamma_s = 0$

4.1.2 Peak Accelerating Voltage for $\dot{B} \neq 0$, $f_s \neq 0$

In order to get the necessary energy gain per turn, one has

$$V \sin \varphi_s \left[kV\right] = 0.020958 \cdot R \cdot \dot{p} \left[\frac{GeV \cdot m}{c \cdot sec}\right], \text{ see } [6, \text{ p. } 31]$$

or with R = 50,42 m :

$$V \sin \varphi_s \left[kV\right] = 1.0567 \cdot \dot{p} \left[\frac{GeV}{c \cdot sec}\right]$$

Furthermore, no reduction of the bucket area due to space charge shall occur. Since there is no explicit expression for the bucket area reduction due to space charge, we use the curves on p. 32 of [6] .

The ordinate units are

$$1 - \frac{A_{sp}}{A} = 1 - \frac{8 \bar{\pi} T \left(\Delta p/p\right)}{16 \beta \chi(\bar{\Gamma}) \sqrt{\frac{e V E}{2 \bar{\pi} h \eta}}}$$

and on the abscissa

$$\Lambda A_{sp} = \frac{4 \bar{\pi} h g_c E_o r_p N}{R e V \gamma^2}$$

(r_p = classical proton radius, N, g_c see previous chapter). The function $\chi(\bar{\Gamma})$ can be found on page 31 of [6], where $\bar{\Gamma} \equiv \sin \varphi_s$ is on the abscissa.

Finally we assume

$$\dot{p} = \text{const.} = 4.5 \frac{GeV/c}{sec}$$

This leads to

$$V \sin \varphi_s = 4.77 \text{ kV}$$

By interpolation using the graphs on pp. 31,32 in [6] , we find V, φ_s, $1 - A_{sp} / A$ as summarized in the following table :

h	V	φ_s	A_{sp} / A
11	6.0 kV	53^o	0.6
22	6.6 kV	46^o	0.5
33	7.2 kV	41^o	0.5

In order to see the difference resulting from not considering space charge, and for two different values of $\dot{p}$, the following two tables are given :

no space charge, $\dot{p} = 4.5 \frac{GeV/c}{sec}$ ($V \sin \varphi_s = 4.77$ kV)

h	V	s
11	5.5 kV	60^o
22	5.8 kV	55^o
33	6.2 kV	50^o

no space charge, $\dot{p} = 2 \frac{GeV/c}{sec}$ ($V \sin \varphi_s = 3.113$ kV)

h	V	s
11	3.6 kV	54.4^o
22	2.8 kV	49.0^o
33	2.9 kV	46.8^o

The momentum spread of the beam at the end of the acceleration can be decreased by reducing the RF-voltage until nearly debunching. If one assumes adiabatic capture and acceleration up to a momentum p_f the final momentum spread with the full

RF-voltage V_{RF} = 5 kV $\Rightarrow (\frac{\Delta p}{p})_f$ and with V_{RF} = 0 $\Rightarrow (\frac{\Delta p}{p})_{fd}$ is given in the following table :

p_f c	$(\frac{\Delta p}{p})_f$	$\Delta \varphi_f$	$(\frac{\Delta p}{p})_{fd}$
2.0 GeV	$2.0 \cdot 10^{-4}$	42.1^o	$2.4 \cdot 10^{-5}$
3.0 GeV	$1.9 \cdot 10^{-4}$	30.8^o	$1.6 \cdot 10^{-5}$
4.0 GeV	$1.9 \cdot 10^{-4}$	21.9^o	$1.2 \cdot 10^{-5}$
4.5 GeV	$2.0 \cdot 10^{-4}$	18.8^o	$1.1 \cdot 10^{-5}$

We get these numbers by a computer program that simulates the adiabatic capture ($dA / A = 0.9\ dt / T_s$, see [2]) of a proton beam with $(\Delta p / p)_i = 5 \cdot 10^{-4}$ bin. It gives us an occupation region of $\Delta \varphi_o = 83^o = 1.45$ and ΔE_o = 25.6 keV at the 3800. revolution and we extrapolated to $\Delta \varphi_f$ and $(\Delta p / p)_f$ by means of

$$\Delta \varphi_f = \Delta \varphi_o \sqrt[4]{\frac{\gamma_o \eta_f}{\gamma_f \eta_o}}$$

and

$$(\frac{\Delta p}{p})_f = \frac{1}{\beta_f \beta_o} \cdot \frac{\Delta E_o}{E_f} \sqrt[4]{\frac{\gamma_f \eta_o}{\gamma_o \eta_f}}$$

4.2 Frequency Range

The accelerating frequency is

$$f_a = h \cdot f_o = h \cdot \frac{c}{2 \pi R_m} \cdot \beta$$

h = harmonic number
f_o = revolution frequency
c = velocity of light
$R_m = \frac{\ell L}{2 \pi}$ = mean orbit radius
L = length of orbit

For the storage rings "DORIS" and the synchrotron "DESY" we have

$$\frac{L_{DESY}}{L_{DORIS}} = 1.1$$

Thus the lowest possible harmonic numbers are

h_{DESY}	11,	22,	33,	...
h_{DORIS}	10,	20,	30,	...

Accelerating protons in DESY from $p_{inj} = 86.7$ MeV/c to $p_{max} = 4.5$ GeV/c with $\dot{p} = \text{const.} = 4.5 \frac{GeV/c}{sec}$, the accelerating frequencies at injection and maximun energy will be :

	h = 11	h = 22	h = 33
f_{inj}	0.958 MHz	1.92 MHz	2.88 MHz
f_{max}	10.2 MHz	20.4 MHz	30.6 MHz

$$\frac{f_{max}}{f_{inj}} = 10.65$$

4.3 Accelerating Devices

For the frequency range listed in the previous chapter there are two possibilities :
ferrite loaded cavities,
drift tubes.

4.3.1 Ferrite Loaded Cavities

The ferrite loading cuts sufficiently down on the dimensions of a $\lambda/2$ or $\lambda/4$ resonant cavity so as to make it fit into a normal straight section of a synchrotron. Moreover, the variation of the RF-electric and magnetic field with length

over the coax-transmission-line-type section of the cavity is small. This coax-line-type section may as well be considered as an inductance the impedance of which is increased by the surrounding ferrite rings by a factor of μr. The ferrite loaded coax line section is resonant with the gap capacitance (plus anode circuit capacitance, + stray capacitance).

All formulae and definitions necessary to determine the characteristic parameters of a ferrite loaded cavity are to be found as well in [6, p. 40]).

The quantity

$$\xi = \mu_r \cdot Q \cdot f$$

is to be found in the manufacturers information on ferrites. For the definition of Q one assumes that the ferrite is used for the inductance of a resonant circuit all losses of which occur only in the ferrite

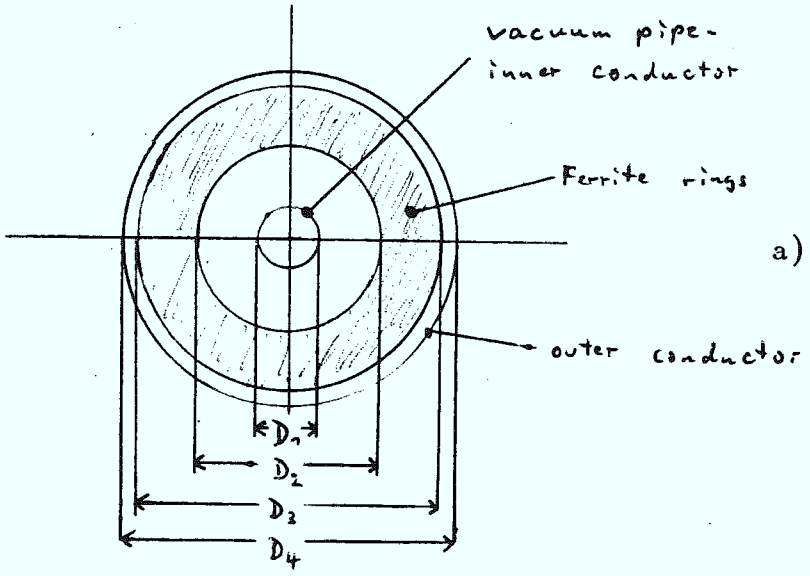

a) cavity cross section

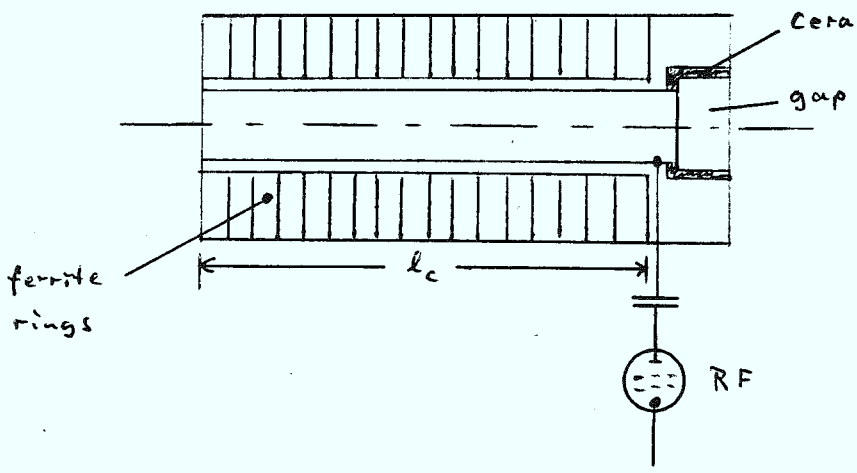

b) ferrite loaded cavity

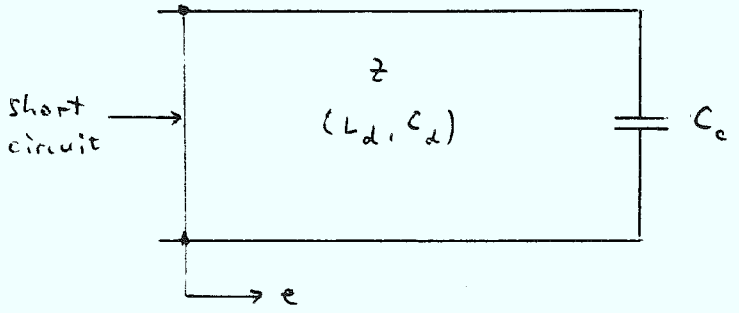

c) equivalent transmission line

The shunt impedance is

$$R_s = \frac{Q}{\omega_0 C} = \frac{2\pi \xi}{\mu_r \omega_0^2 C}$$

In order to adjust the cavity resonant frequency to the accelerating frequency the ferrite will be biased thus changing the μ_r :

$$f^2 \sim \frac{1}{\mu_r} .$$

μ_r is at maximum when unbiased for low frequency at the beginning of acceleration, and at minimum when fully biased for high frequency at the end of acceleration. With

$$\gamma = \frac{f_{max}}{f_{inj}} = 10{,}65$$

$$\gamma^2 = \frac{u_{r\ max}}{u_{r\ min}} = 114$$

The peak dissipated power per volume unit is

$$(*)\ \hat{P}' = \frac{\hat{V}^2}{4\pi \int \mu_0 A^2}$$

with $\hat{V}$ = peak accelerating voltage

A = flux area = $\frac{1}{2} (D_3 - D_2) l_c$

In order to safe time one would choose ferrite rings already manufactured for CERN:

		4 H 2	4 L 2
D_3	outer diameter	35.0 cm	44.0 cm
D_2	inner diameter	20.0 cm	25.0 cm
d	thickness	3.0 cm	3.3 cm
μ_r	unbiased	230	210

Since it is not possible to cover the entire frequency range with one device only, we split the frequency range in two equal subranges :

$$\frac{\mu_{max}}{\mu_{min}} = \frac{\mu_{max}}{\mu^*} \cdot \frac{\mu^*}{\mu_{min}}$$

$$\frac{\mu_{max}}{\mu^*} = \frac{\mu^*}{\mu_{min}} = 10.65$$

For these two ranges one assumes

$$\xi = \mu_r Q \cdot f \neq F(f)$$

Furthermore the maximum power density in the ferrite shall be

$$\hat{P}'_{max} = 0.2 \left[\frac{W}{cm^3}\right]$$

To find the minimum ferrite length not to exceed the maximum power density we use the formula (*) on page 14

$$\frac{\hat{V}^2}{4\pi^2 \xi \mu_o \hat{P}'_{max}} = (R_3 - R_2)^2 \, l_c^2$$

$$l_{min} = \frac{2\,\hat{V}}{(R_3 - R_2)\sqrt{\mu_o \pi \hat{P}'_{max}}} \cdot \frac{1}{\sqrt{\xi}}$$

For different flux densities B_{RF} we find $\xi = \mu \cdot Q \cdot f$ from the ferrite measurements done at CERN ($\mu \cdot Q$ vs B_{RF} at f = 2.5 MHz) (see Fig. 11). With these values we get l_{min} as a function of B_{RF} as shown in Figs. 12a, 12b, 12c for h = 11,22,33 and for the two ferrites 4 H 2 and 4 L 2.

Furthermore the peak accelerating voltage V will cause a peak RF induction $\hat{B}_{RF}$ which also depends on the ferrite structure length.

$$\hat{B}_{RF} = \frac{\hat{V}}{\omega A} = \frac{\hat{V}}{2\pi f (R_3 - R_2)\, l_c} = \frac{\text{const}}{l_c}$$

$\hat{B}_{RF} = F(l_c)$ for the two ferrites, and h = 11, 22, 33 is also shown in Figs. 12a, 12b, 12c. We obtain the following numbers

		h = 11		h = 22		h = 33	
total frequ.swing (MHz)		0.95..10.2		1.92..20.4		2.88..30.6	
cavity I	frequ.swing (MHz)	0.95 ..3.1		1.9 .. 6.3		2.7 .. 9.4	
	type of ferrite	4H	4L	4H	4L	4H	4L
	l_{min} (cm)	70	70	65	36	70	39
cavity II	frequ.swing (MHz)	3.1 ..10.2		6.2 ..20.4		9.3 ..30.6	
	type of ferrite	4H	4L	4H	4L	4H	4L
	l_{min} (cm)	42	23	43	21	47	23

Since the ferrites 4 H and 4 L were designed for the frequency range 1 MHz ... 10 MHz, the assumption $\xi \neq F(f)$ is no longer valid at least for the numbers listed under h = 33.

Without bellows, the available space in the azimuthal direction in a DESY straight section is 174 cm, with bellows 142 cm. The ferrite length of a half-cavity therefore should not exceed 60 cm.

The RF power is for two half cavities

$$\hat{P} = \hat{P}' \cdot Vol = \frac{\hat{B}^2 \omega^2}{4\pi\mu_o \zeta} \cdot Vol$$

Choosing e.g. h = 22 and ferrite type 4L we get the following quantities :

Cavity I :

l_c	= 36	[cm]
B_{RF}	= 158	[T]
$\zeta = \mu_{eff} \cdot f$	= $1.5 \cdot 10^{10}$	[sec^{-1}]
μ_r	= 320	
μ_{eff}	= 122	
$\hat{P}'$	= 0.15	[W/cm^3]
Vol	= $2.42 \cdot 10^4$	[cm^3]
$\hat{P}$	= 3.62	[kW]

For resonance, the additional gap capacitance is about 400 pF.

Cavity II :

l_c	= 21	[cm]
B_{RF}	= 85	[T]
ζ	= $4.5 \cdot 10^{10}$	[sec^{-1}]
μ_r	= 250	
μ_{eff}	= 95	
$\hat{P}'$	= 0.154	[W/cm^3]
Vol	= $1.41 \cdot 10^4$	[cm^3]
$\hat{P}$	= 2.18	[kW]

For resonance, the additional gap capacitance is about 50 pF.

We have to remind that the CERN ferrite measurements were done at 2.5 MHz and 10 MHz. So we are not sure how wrong e.g. the assumption $\zeta \neq F(f)$ will be at frequencies much higher than 10 MHz.
The total ferrite length
l_{tot} = 2 x 36 cm + 2 x 21 cm = 114 cm
would allow to locate both cavity I and cavity II in one synchrotron straight section with the remaining space
144 cm - 114 cm = 30 cm to be used for the gaps and flanges, see Fig. 13.

4.3.2 Radio Frequency Acceleration with Drift Tubes

For a drift tube, however, the voltages across the two gaps are out of phase. The gap voltage is given by

$$\hat{V}_{gap} = \frac{\hat{V}_{acc}}{2 \sin \varphi/2}$$ (see Fig 14 a, b)

with $\hat{V}_{acc}$ = peak accelerating voltage and

$\varphi = \omega \Delta t = 2 \pi f \, l_d / \beta c$

For small φ

$$\hat{V}_{gap} = \frac{\hat{V}_{acc} \, R}{h \, l_d}$$

Compared to the RF cavity, drift tube RF acceleration has the disadvantage of high gap voltages and high RF power. However, the ferrite choke determining the frequency can be located aside from the accelerating structure allowing ample space for a high number of windings.

4.4 Data of the PPA Accelerating Unit

It would be helpful for us if we could install the PPA accelerating unit, may be with some modifications, in our synchrotron to save time and money.
The data of the PPA accelerating unit are the followings :

The PPA rf accelerating unit is a composite of a cavity and a drift tube system.

Frequency range of composite system	2.5 ... 30.0 MHz
frequency range of drift tube system	2.5 ... 7.0 MHz
frequency range of cavity	6.5 ... 30.0 MHz
total length of drift tube	1.54 m

the maximum drift tube voltage V_{gap} is reported to be 2o kV (see [8]).

For DESY application we need :

	V_{acc} kV	V_{gap} kV	P kW
h = 11	10	29.9	20
h = 22	13	19.7	17.4
h = 33	16	16.6	18.2

These numbers are based on a drift tube total capacitance of C = 600 pF and of a ferrite Q-value of 80 *.

For the cavity, the frequency range was

6.5 ... 30 MHz

calling for variation in μ :

$$\eta^2 = \left(\frac{30}{6.5}\right)^2 = 21 = \frac{\mu_{max}}{\mu_{min}}$$

This requires $15 \cdot 10^3$ A bias current. At PPA, a transformer is used, since the machine is cycling with 20 per sec.. At DESY with a cycle of less than 1 per sec, the frequency range will have to be split up.

If we choose h = 33 the magnetic field for the drift tube tuning could easily be made higher by adding a few windings (the inductance is an external choke set up from 4 ferrite rings). This would increase the drift tube system frequency range, thus allowing to decrease the cavity system frequency range. E. g. splitting up the total frequency range

2.7 ... 30.6 MHz

into equal ranges

2.7 ... 9.4 MHz drift tube system

9.3 ... 30.6 MHz cavity system

would bring down the μ-variation of the cavity system to

$$\eta^2 = 11$$

since μ is roughly proportional to $1 / I_{bias}^2$

$$\eta^2 = 11 \Rightarrow I_{bias,max} = 15 \sqrt{11/21} \cdot 10^3 \text{ A} = 10.8 \cdot 10^3 \text{ A}$$

Still, $\sim$ 11 kA is a high quantity. Instead of trying to push the drift tube system high frequency end even higher one might consider to split up the cavity system frequency range:

drift tube system frequency swing :	2.5 ... 6.5 MHz
cavity system frequency swing (I) :	6.5 ... 13.9 MHz
cavity system frequency swing (II):	13.9 ... 30.6 MHz

Since the PPA system incorporates 2 cavities each cavity might be given its own frequency range ($\eta = 2.14$; $\eta^2 = 4.6$).

---

* The necessary accelerating voltages V_{acc} were calculated originally with the assumption of a momentum spread of $\Delta p/p = 4 \cdot 10^{-3}$ bin in the injected beam.

5. The Magnet Circuit for Proton Acceleration.

5.1 Modification of Magnet Cycle

For the normal 50 cps - operation and for a peak momentum of 4 GeV / c the maximum accelerating voltage is

$$V \sin \varphi_s \left[kV \right] = 1.0567 \, \dot{p}_{max} \left[\frac{GeV/c}{sec} \right]$$

Thus

$$(V \sin \varphi_s)_{max} = 660 \text{ kV}$$

For $\varphi_s = 45^o$: V = 935 kV.

For electron acceleration, a megavolt per turn is no problem because of the high shunt impedance of fixed frequency rf-cavities. For ferrite loaded variable frequency proton rf-accelerating cavities, the shuntimpedance per gap is by 3 of magnitude lower. From this it is obvious, that the magnet cycle time must be drastically increased. In principle, this could be achieved with a magnet circuit resonant at a very low frequency, say 1 Hz.
However, this would mean a lot of additional hardware (capacitors, switches), since the accelerator must be switched from proton acceleration to electron acceleration within a short time (a few minutes). So one would try to program the ignitron-controlled existing magnet dc-power supply. Special attention has to be paid to what happens right at the moment where the current ramp starts (i.e. when the powersupply generates a voltage " step ").

First, too fast change in current will cause closed orbit distortions because of transients in the magnet circuit (so called " transmission line modes "),
second, for a " smooth " start of the ramp, a compromise will have to be found in order to avoid particle losses due to gas scattering.

5.1.1 Limits dtermined by the Present DC-Power Supply (see Fig.15)

The ignitron - contolled powersupply is capable of

1.1 kV max

680 A max

The inductance and resistance of the magnet circuit will be (see Fig.20a, switches closed)

L = 1.5 H

R ≈ 1.0 Ω

From this the maximum rate of increase for the magnet current is

$$\left|\frac{\Delta I}{\Delta T}\right|_{max} = 730\left[\frac{A}{sec}\right] \hat{=} \dot{p} = 4.4\left[\frac{GeV/c}{sec}\right]$$

Because of the special properties of the internal control feedback circuits, and the filter circuits, a practical limit will be

$$\dot{p}_{max} = 3.5\ \frac{GeV/c}{sec}$$

For details, see Fig. 16.

The maximum momentum rise as mentioned above will be sufficient for a maximum momentum of 2.2 GeV/c (present stage of fast ejection from the synchrotron, and beam transport to the storage rings). For higher maximum momentum (up to 5 GeV/c), the rate of rise will have to be considerably larger. After the first storage ring improvement program (upgrading of energy to max 5 GeV) will be finished, a power supply capable of

2.5 kV

1.5 kA

will be available for the synchrotron magnet, allowing rise times faster by more than a factor of 2.

5.1.2 Rearrangement of the Magnet Circuit

Switchover from electron/positron to proton operation - and back - must be achieved within a few minutes. In the proton case the choke windings are not needed. In order to decrease the entire circuit inductance, the secondary windings of the choke can be shorted out

by switches S_1 ... S_{12} (see Fig. 17a).
However, the long cables between the magnet groups (L_{Mn} in Fig. 17a) located in the synchrotron tunnel and the capacitor groups C_n located outside the accelerator building, and the main choke itself cause large capacitance to ground.
For transient conditions, large currents may flow across this capacitance disturbing the symmetry in space of the whole magnet circuit, resulting in differences in the magnet field of one magnet group compared to the others. If it should turn out, that this problem cannot be handled otherwise, the synchrotron magnets (for proton acceleration) could be connected directly by special switches located in the tunnel (see Fig. 17b).

5.2 Influence of Capacitive Leak Currents to Ground on the Synchrotron Closed Orbit

Leak currents to ground will cause differences of excitation for the synchrotron magnets and thus closed orbit deformations. Estimations on these closed orbit deformations lead to the following relation :

$$\hat{x}_c \left[m \right] = 7.5 \frac{\Delta B}{B}$$

with $\hat{x}_c$ the max. statistical orbit deviation in closed magnets.
The acceptance reduction due to this deviation is given by

$$\frac{\Delta \varepsilon}{\varepsilon_o} = \frac{2 \hat{x}_c}{\sqrt{\varepsilon_o \beta}}$$

and thus

$$\frac{\Delta B}{B} = \frac{\sqrt{\varepsilon_o \beta_F}}{15} \frac{\Delta \varepsilon}{\varepsilon_o}$$

If we assume $\varepsilon_o \approx 60$ mm·mrad, and $\beta_F = 21$ m, and regard 10 % loss of acceptance as tolerable, the max. statistical field error will be

$$\frac{\Delta B}{B} = 2.4 \cdot 10^{-4}$$

5.3 Measurements on Errors of the Injection Field due to the Transient at the Current Ramp Start

The magnet equivalent circuit is a "transmission line" with the magnets as inductances and the stray capacitance against ground as capacitors (see Fig. 17a). For calculations, however, it is difficult to get sufficiently exact results on what happens around the magnet ring when a voltage step is applied at the normal dc feed-in point, because of the uncertainty on the exact quantities of the distributed circuit elements. Therefore measurements were done in the actual circuit. First results are available for the two possibilities indicated by the Figs. 17a and 17b. Fig. 18 demonstrates the set up used for the measurements.
The results of several measurements done on different occasions are listed in the table below, using the following quantities :

V_N	voltage applied to the magnet circuit at the normal dc-power input point
$\frac{\Delta V_N}{\Delta t}$	rise of V_N with time
V_M	integrator output voltage
R_p	damping resistors
ΔI	difference of exciting currents in the two magnets compared in the measurements
$\frac{\Delta B}{B_{inj}}$	difference of field between magnet groups 1 and 12, related to the proton injection magnetic field
τ_1	time necessary for V_N to reach its max value of 1.1 kV
τ_2	time constant as measured for the decrease of the transmission line response to V_N
f	frequency of the oscillation contained in the transmission line response to V_N

Measurement No.	1	2	3	4	5	6	7	8
circuit Fig. 17	a	a	b	a	a	a	a	a
R_p [Ohm]	-	-	-	-	-	270	270	-
$\frac{V_N}{t}$ [$\frac{V}{msec}$]	90	47	84	140	5.5	7.5	2.7	45
I [mA]	490	180	31	280	19	36	4,3	108
$\frac{B}{B_{inj}}$ [%]	3.4	1.25	0.22	1.9	0.13	0.25	0.03	0.75
τ_1 [msec]	12	24	13	8	200	147	400	25
τ_2 [msec]	-	-	-	30	30	6	-	-
f [Hz]	-	-	3750	185	190	185	-	-

From Fig. 19 we learn, that the accuracy of the measurements is not very good since the relative field errors $\Delta B/B_{inj}$ depending on the voltage rise time $\Delta V_N/\Delta t$ measured on different occasions are relatively far from being positioned on a straight line. However, within a factor of 2 uncertainty we can derive now the relationship between $\Delta V_N / \Delta t$ and the relative field error between magnetgroup 1 and 12 :

$$\frac{\Delta V_N}{\Delta t}\left[\frac{V}{msec}\right] \cong 50 \frac{\Delta B}{B}[\%]$$

Further measurements had shown that the field error will rise linearly with the magnet group number. Under these conditions the calculated closed orbit will have a max. amplitude of

$$\pm 22 \text{ mm with } \Delta B / B = 1\%$$

for the magnets adjacent to the circuit input. If we tolerate a closed orbit deviation of $\pm$ 5 mm, then

$$\frac{\Delta V_N}{\Delta t} = 12 \left[V/msec\right]$$

Since V_N = 950 V is necessary for a momentum rise of 3.5 $\frac{GeV/c}{sec}$ it follows that 80 msec is the minimum rise time.
See Fig. 20 for the current and voltage functions with time.
The closed orbit deviations due to the transient at the "current ramp" beginning could be kept smaller by re-arranging the synchrotron magnet circuit considerating betatron phase conditions. However, this would mean a big effort in terms of time, manpower and money.
The circuit as shown in Fig. 17b would permit a much faster rise time

$$\frac{\Delta V_N}{\Delta t} \approx 87 \left[\frac{V}{msec}\right] \quad (\pm 5 \text{ mm closed orbit deviation}).$$

6. Vacuum - Requirements

The number of the protons in the synchrotron are limited essentially by two effects:

1. The ΔQ - shift due to space charge and
2. the multiple Coulomb scattering in the residual gas leading to particle loss at the walls of the vacuum chamber.

The maximum currents and numbers of particles limited by space charge were calculated according to the Laslett formula [6, page 26] and are given for different emittances of the injected beam in the following table:

ε_o [rad m]	$\varepsilon_o \beta\gamma$ [rad m]	i [mA]	N
$6 \cdot 10^{-6}$	$0.55 \cdot 10^{-6}$	0.9	$6 \cdot 10^{10}$
$15 \cdot 10^{-6}$	$1.38 \cdot 10^{-6}$	2.2	$16 \cdot 10^{10}$
$30 \cdot 10^{-6}$	$2.76 \cdot 10^{-6}$	3.9	$28 \cdot 10^{10}$

The emittance growth due to the restgas is given by

$$\Delta(\varepsilon\beta\gamma) = \frac{\beta_s \, 15^2 \, c \, P\,[\text{Torr}]}{291 \cdot 760 \cdot E_o^2} \int_{(T)} \frac{dt}{\beta^2 \gamma}$$

This emittance growth was calculated versus time for a momentum rise according to Fig.20 .

There is first an increase of the unnormalised emittance due to the restgas scattering and than a decrease due to the adiabatic damping. The resulting maximum emittance was compared with the acceptance of the synchrotron ($\approx 30\ \pi$ mm mrad). The maximum currents for different pressures P Torr and for different emittances ε_o of the injected beam are given in the following table :

P Torr	$\varepsilon_o = 6 \cdot 10^{-6}$ radm	$\varepsilon_o = 15 \cdot 10^{-6}$ radm	$\varepsilon_o = 30 \cdot 10^{-6}$ radm
10^{-6}	I = 0.35 mA	I = 0.83 mA	I = 1.43 mA
10^{-7}	I = 0.75 mA	I = 1.63 mA	I = 2.54 mA
10^{-8}	I = 0.88 mA	I = 1.83 mA	I = 2.72 mA

It is obvious that the pressure has to be less than 10^{-7} Torr but we will not gain much more accelerated protons by reducing the pressure another factor of ten.
The pressure at present is $2 \cdot 10^{-7}$ Torr in the synchrotron.

Acknowledgement:
We would like to thank Dr. R. D. Kohaupt for many helpful discussions.

References

1 H.Gerke,H.Wiedemann,B.H. Wiik,G.Wolf
Ein Vorschlag,DORIS als e-p Speicherring zu benutzen.
Int.Bericht DESY H-72/22

2 H.Wiedemann,B.H.Wiik:An Improved Mode of Operation of the proposed DESY e-p Colliding Beam Experiment
Int.Bericht DESY F35 - 72/3

3 A.Febel,H.Gerke,G.Hemmie,H.Kumpfert,M.Tigner,H.Wiedemann, B.H.Wiik: The DESY Synchrotron as a Proton Injector for DORIS
Int.Bericht DESY F 35, H , S1 - 73/1

4 G.W.Wheeler:Experience gained from the New U.S. Linear Accelerators,
Proc.of the 8th Int.Conf.on High Energy Particles,CERN 1971

5 Herb,NEC, private communication

6 C.Bovet,R.Gouiran,I.Gumowski,K.H.Reich
A Selection of Formulae .....,CERN/MPS-SI/Int. DL/70/4

7 C.G.Lilliequist,K.R.Symon:Deviations from Adiabatic Behavior during Capture of Particles
MURA - 491,1959

8 M.Tigner , private communication

9 I.Gumowski,K.H.Reich:Synchrotron Motion in the Presence of Space Charge, CERN SI/Int. DL/70/6 1970

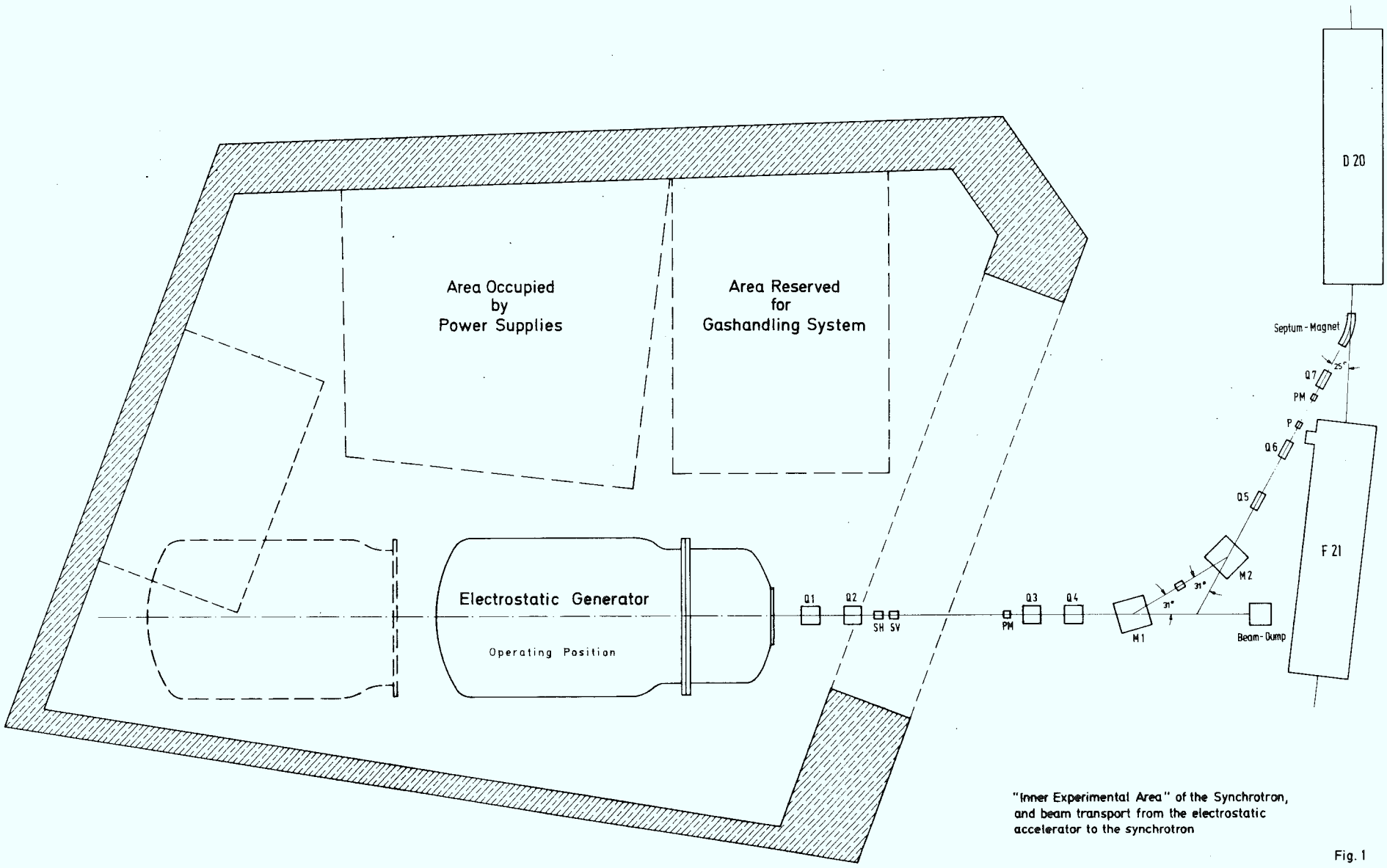

"Inner Experimental Area" of the Synchrotron, and beam transport from the electrostatic accelerator to the synchrotron

Fig. 1

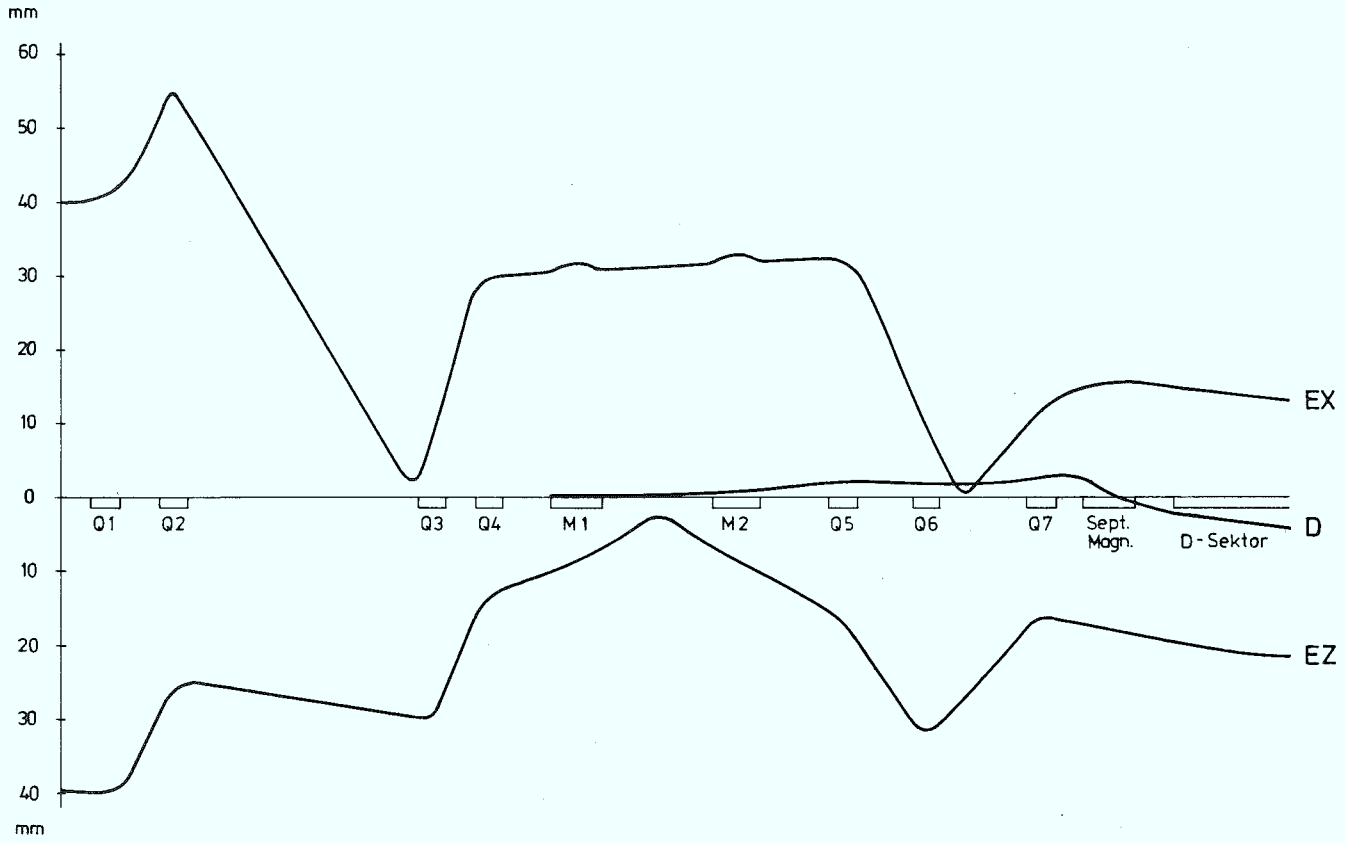

Beam Transport Between Elektrostatic Proton Accelerator and Synchrotron,
Optic for Small Energie Spread

Fig. 2

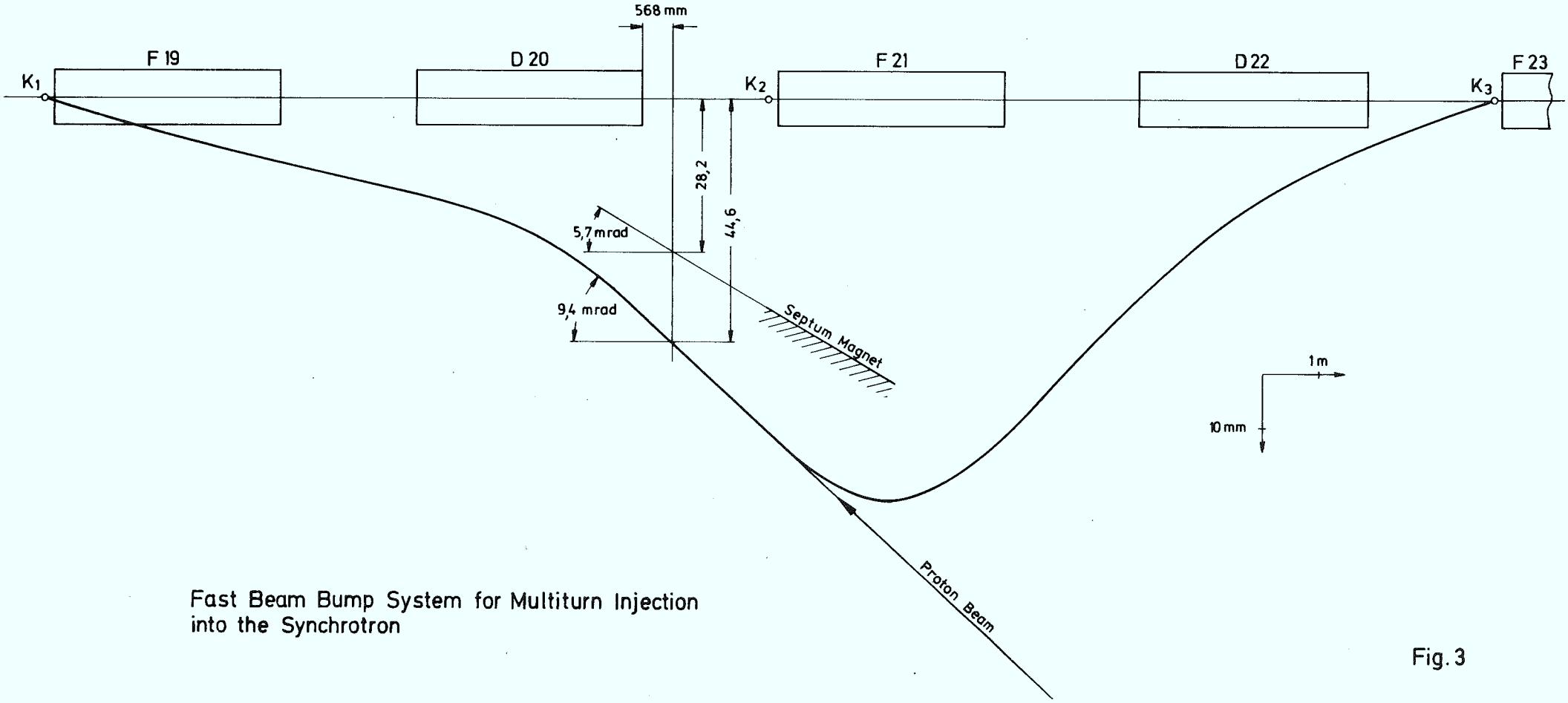

Fast Beam Bump System for Multiturn Injection into the Synchrotron

Fig. 3

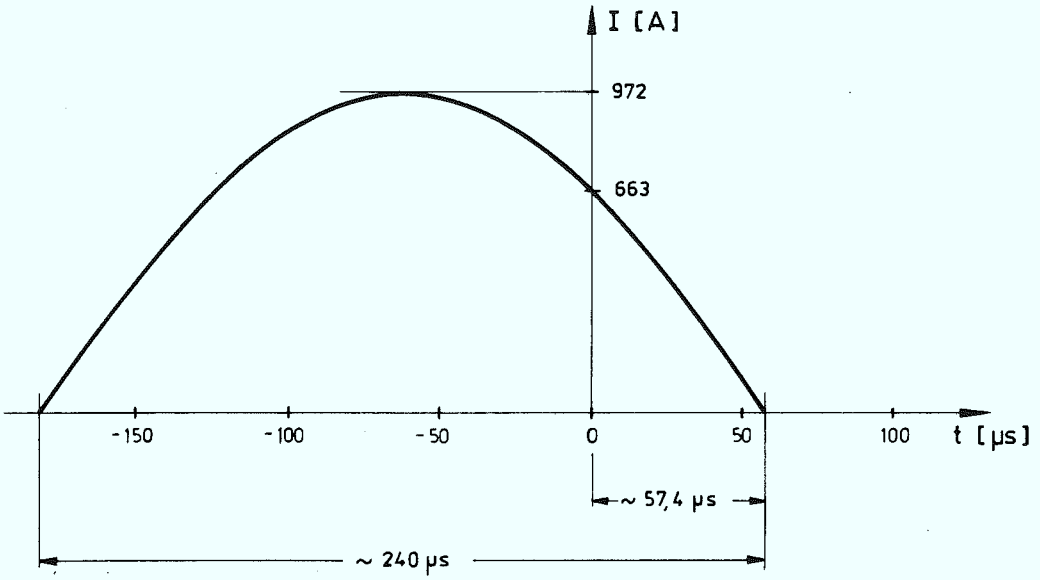

Fig. 5

Current versus time for
fast injection beam bump

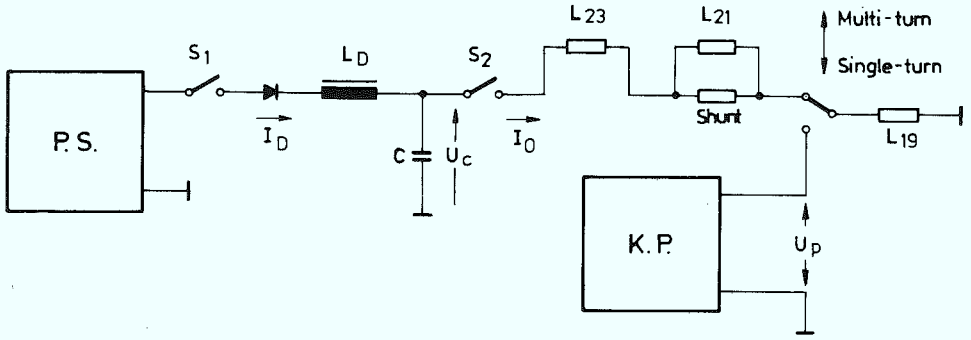

Pulser circuit for fast injection beam bump Fig. 6

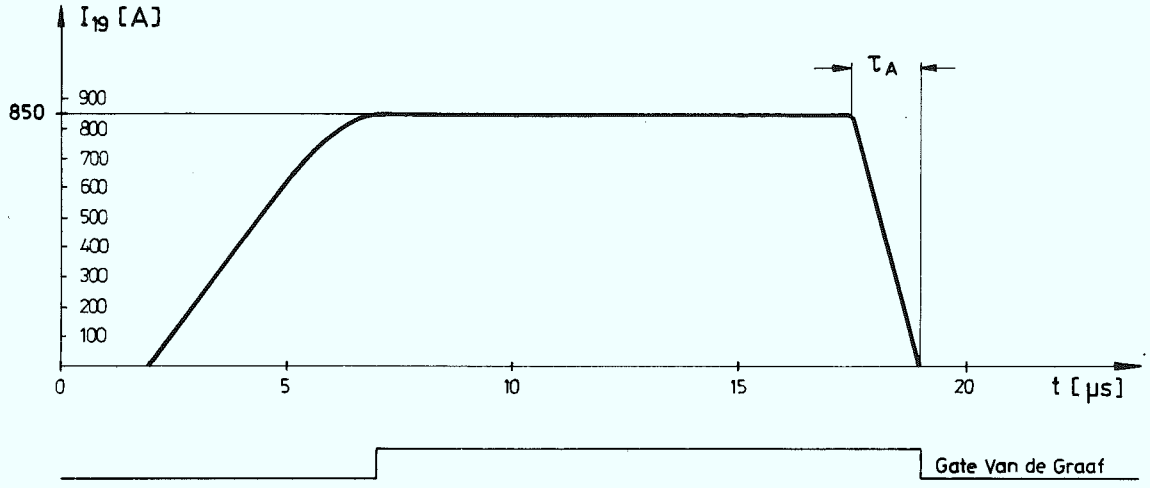

Current (field) versus time in fast kicker for single-turn injection

Fig.7

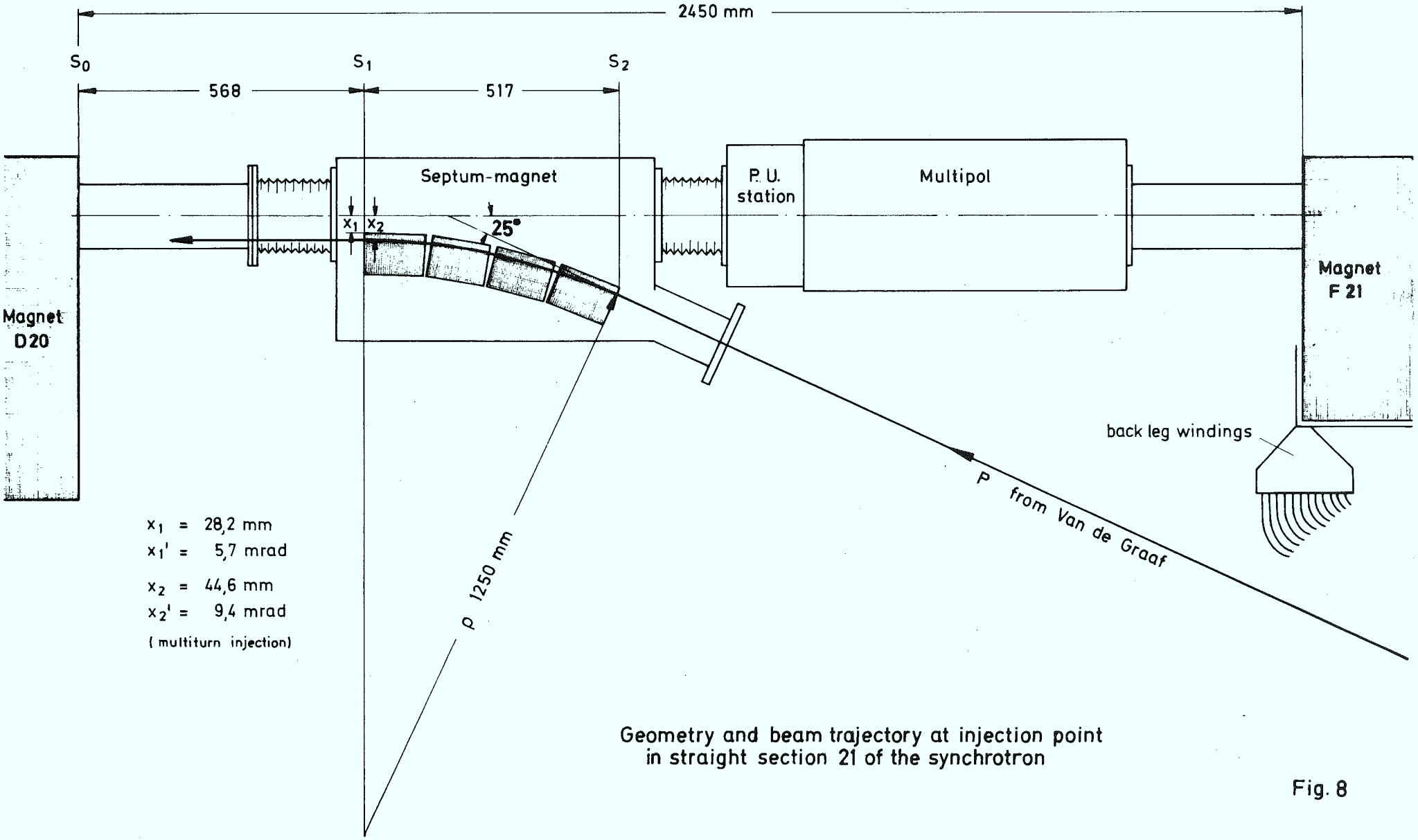

Geometry and beam trajectory at injection point in straight section 21 of the synchrotron

Fig. 8

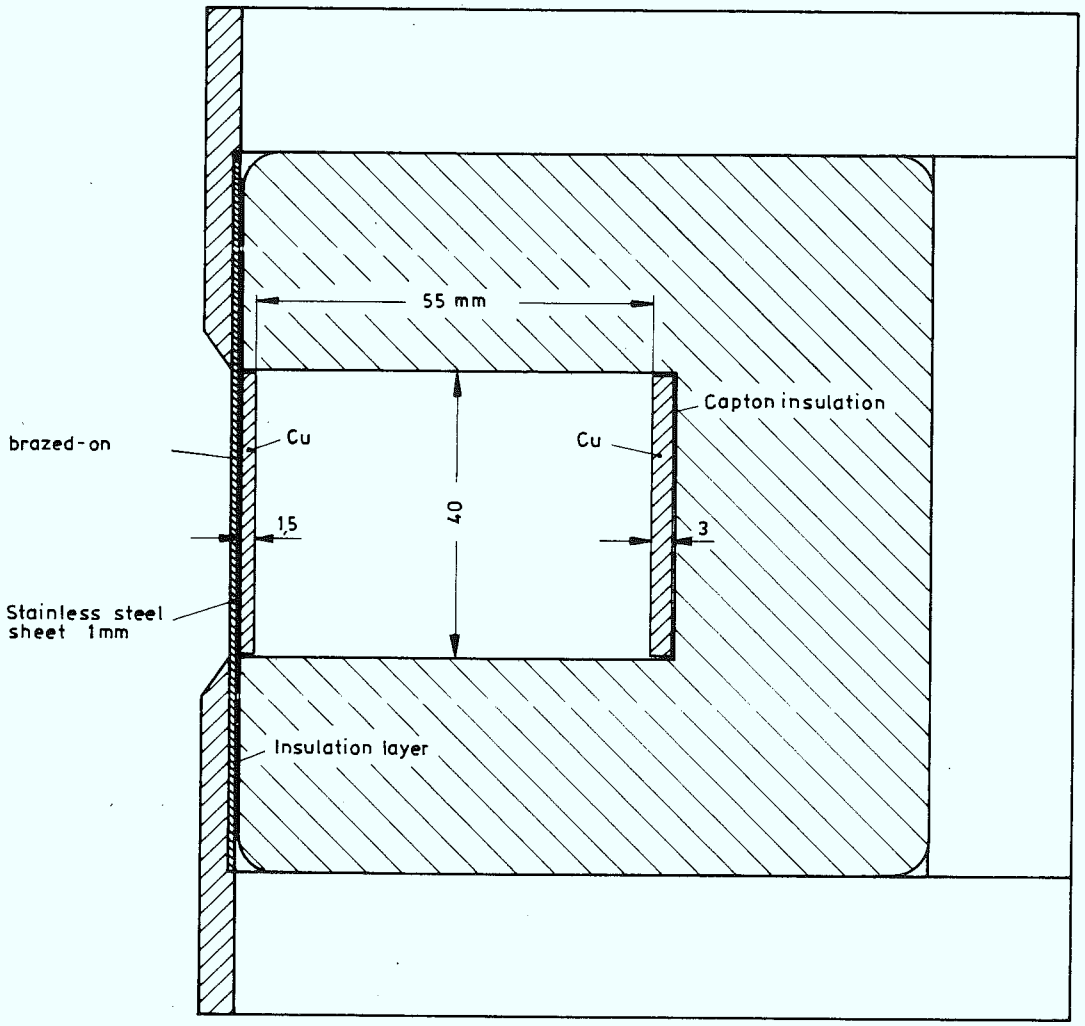

Septum magnet for p-injection
cross section

Fig. 9

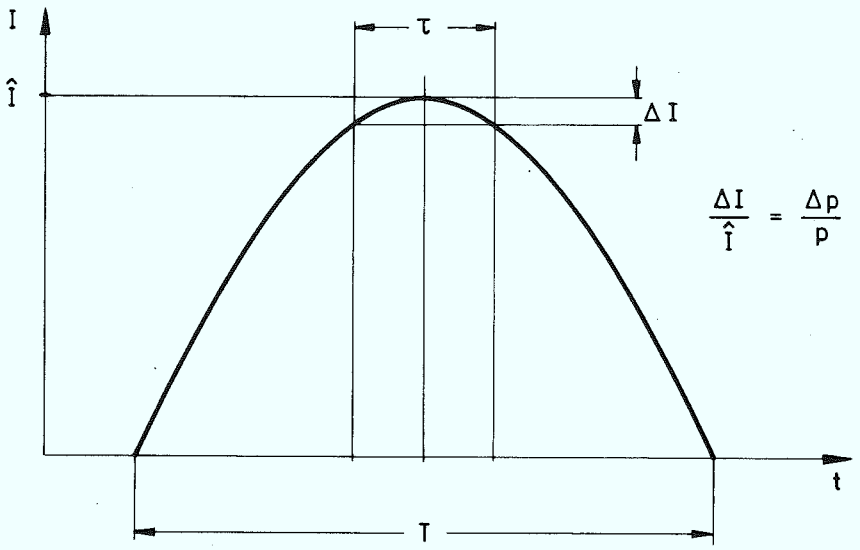

Fig. 10

Sine half-wave current pulse for injection septum

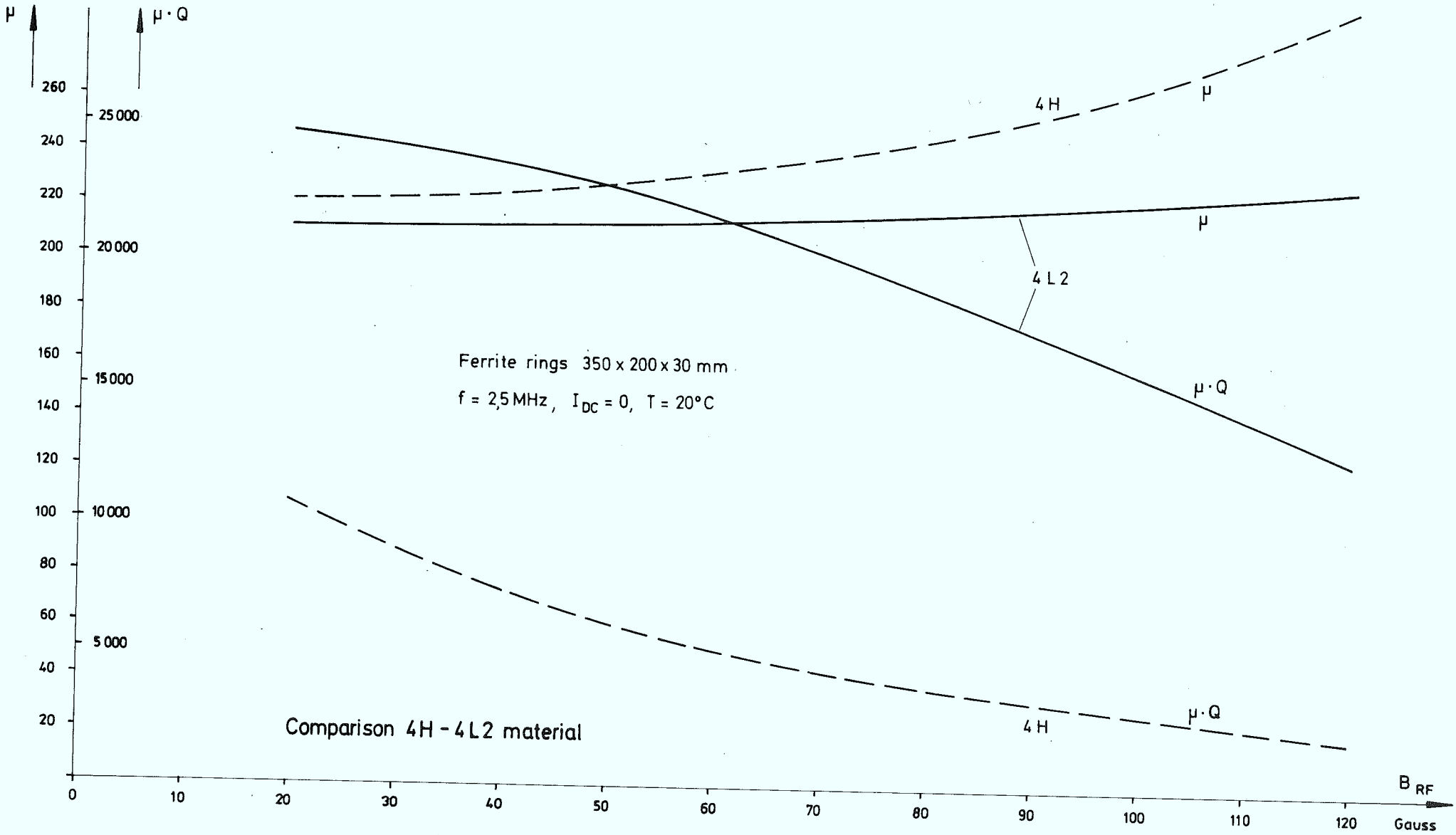

CERN ferrite measurements μQ and μ versus B_{RF}

Fig. 11

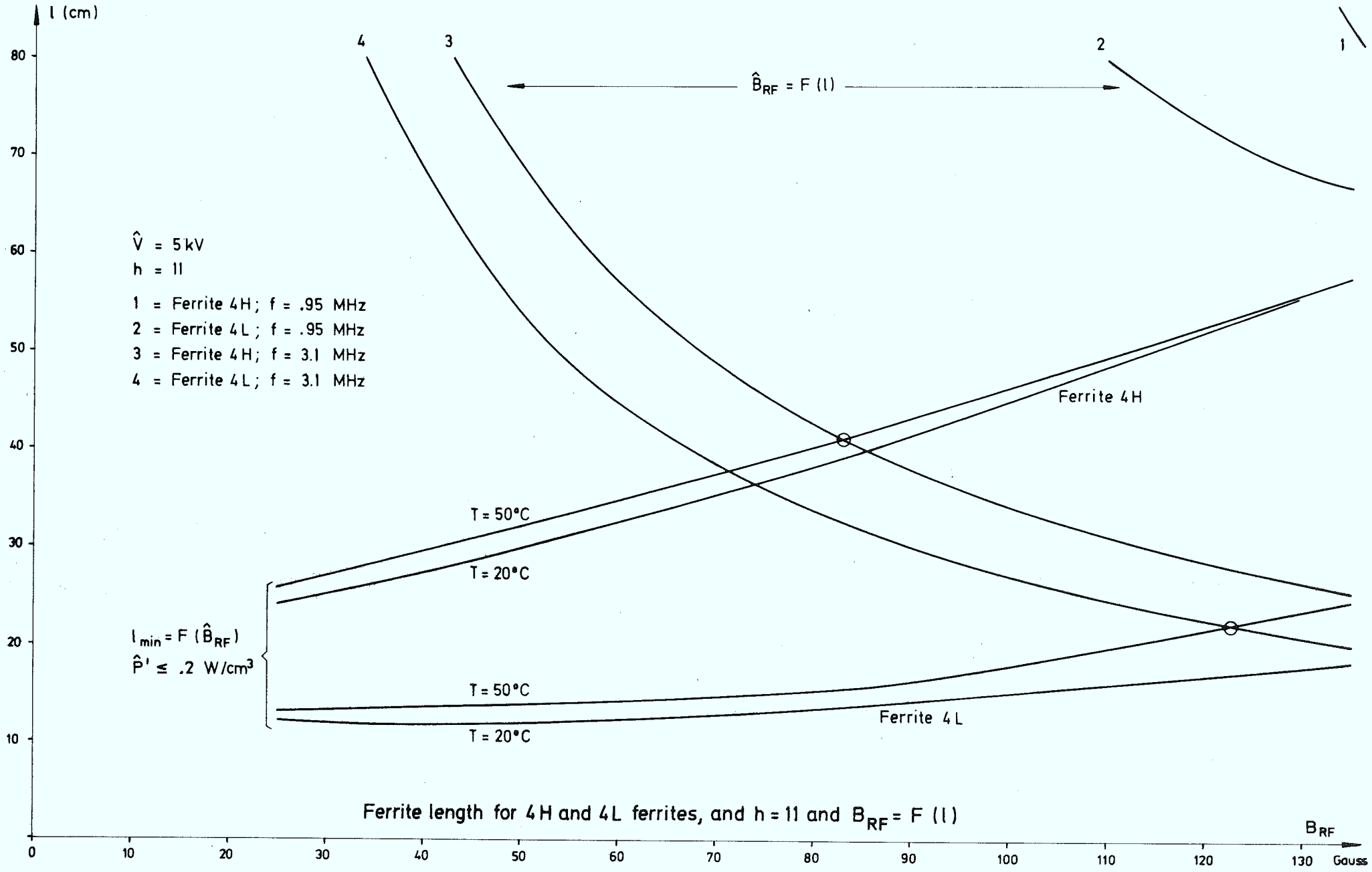

Ferrite length for 4H and 4L ferrites, and h = 11 and $B_{RF} = F(l)$

Fig. 12a

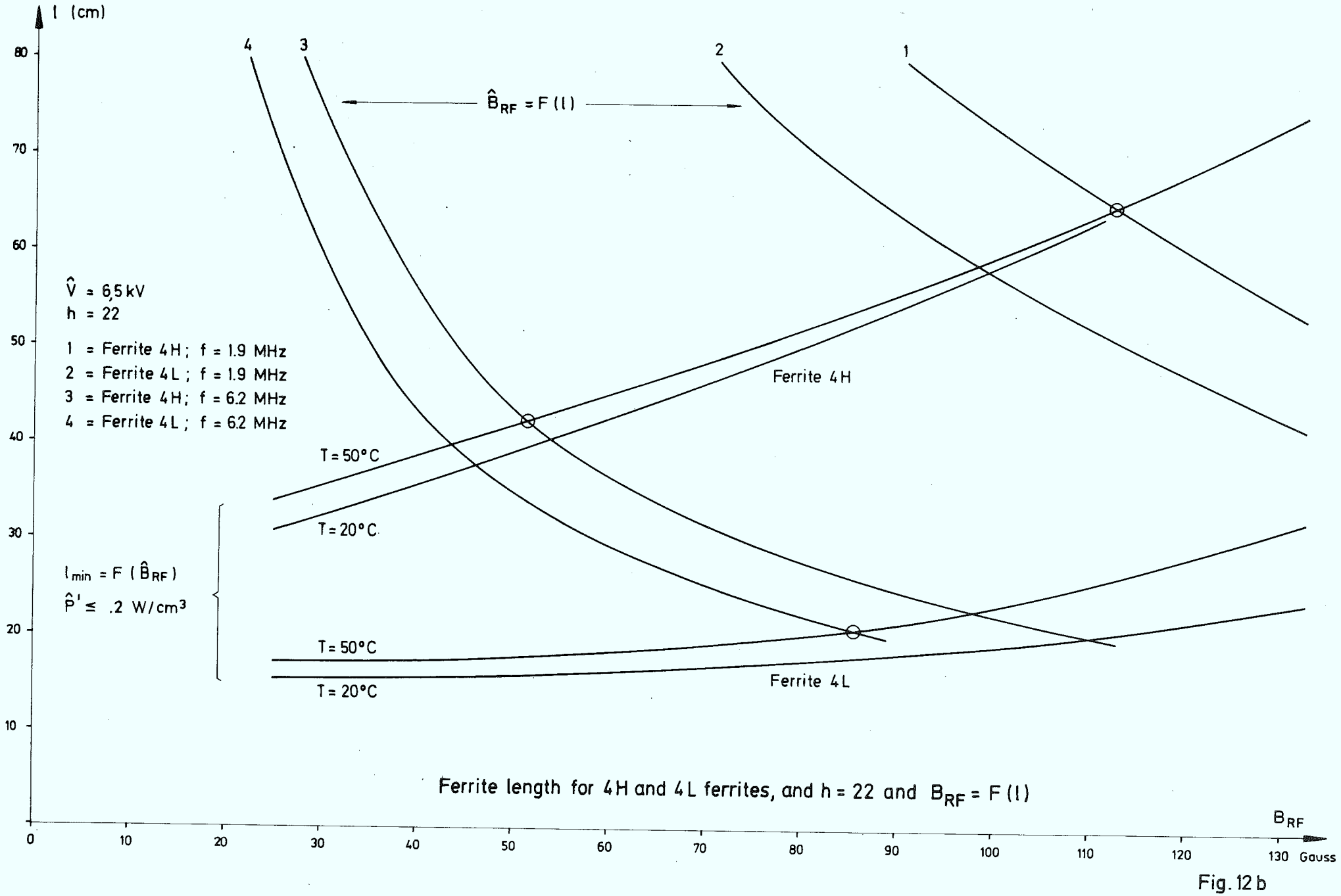

Ferrite length for 4H and 4L ferrites, and h = 22 and $B_{RF} = F(l)$

Fig. 12 b

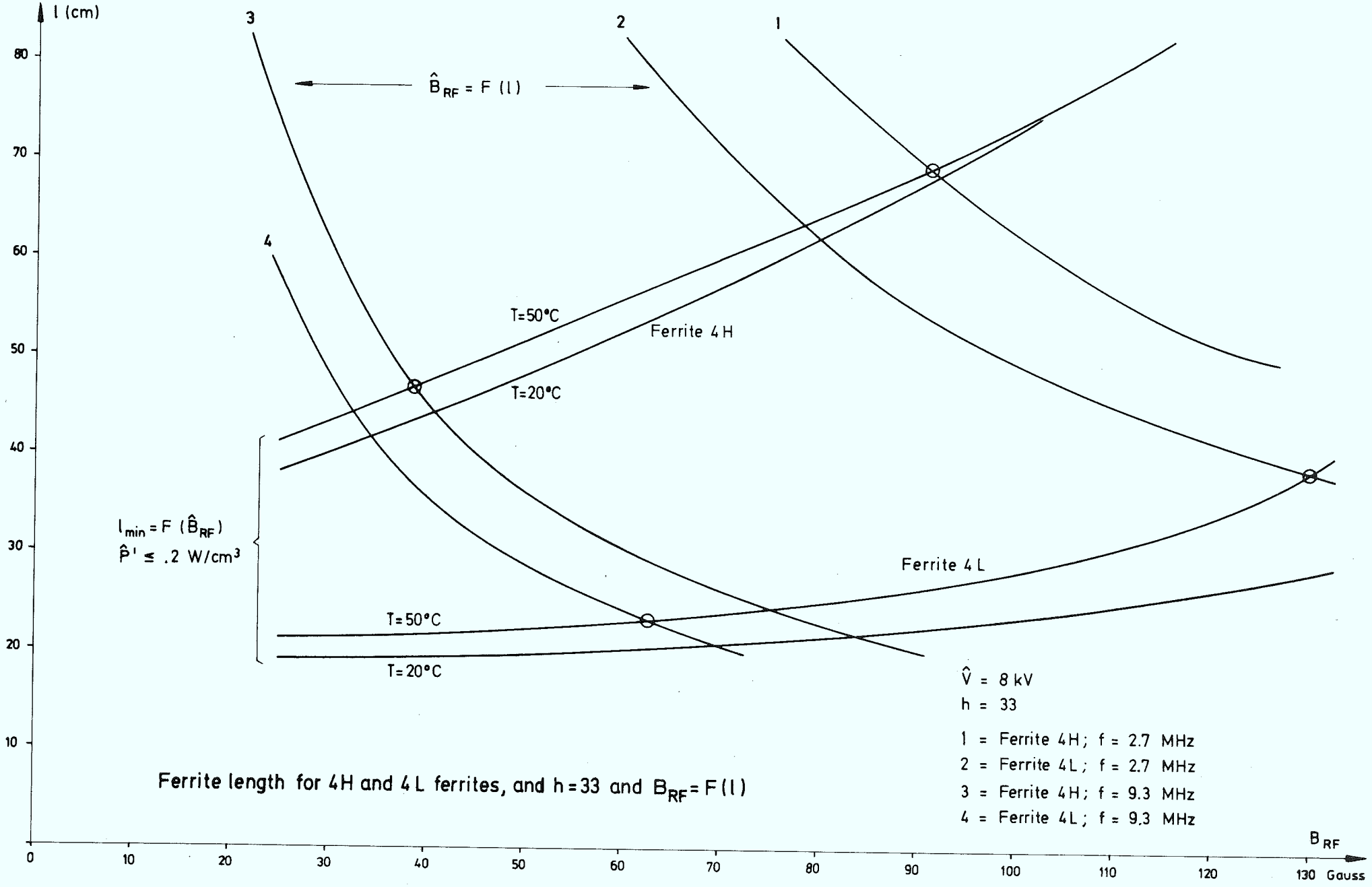

Ferrite length for 4H and 4 L ferrites, and h=33 and $B_{RF} = F(l)$

Fig. 12c

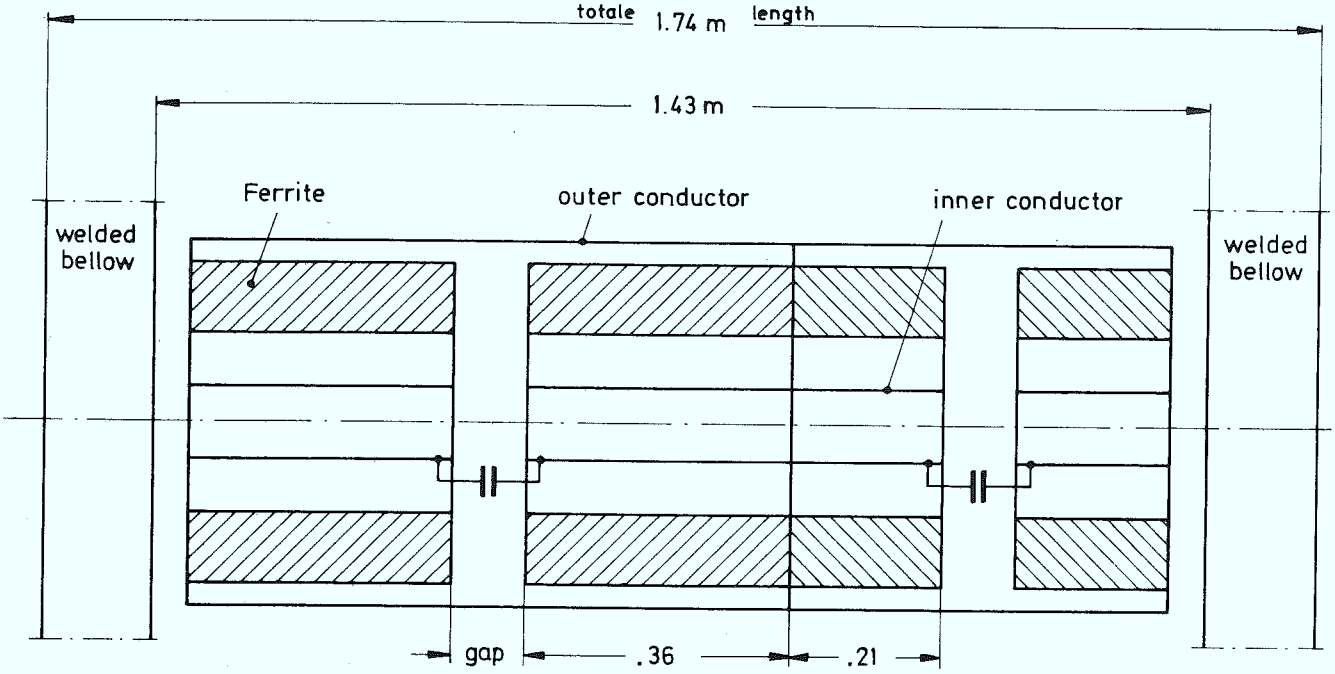

Dimensions of double cavity (two frequency ranges)

Fig. 13

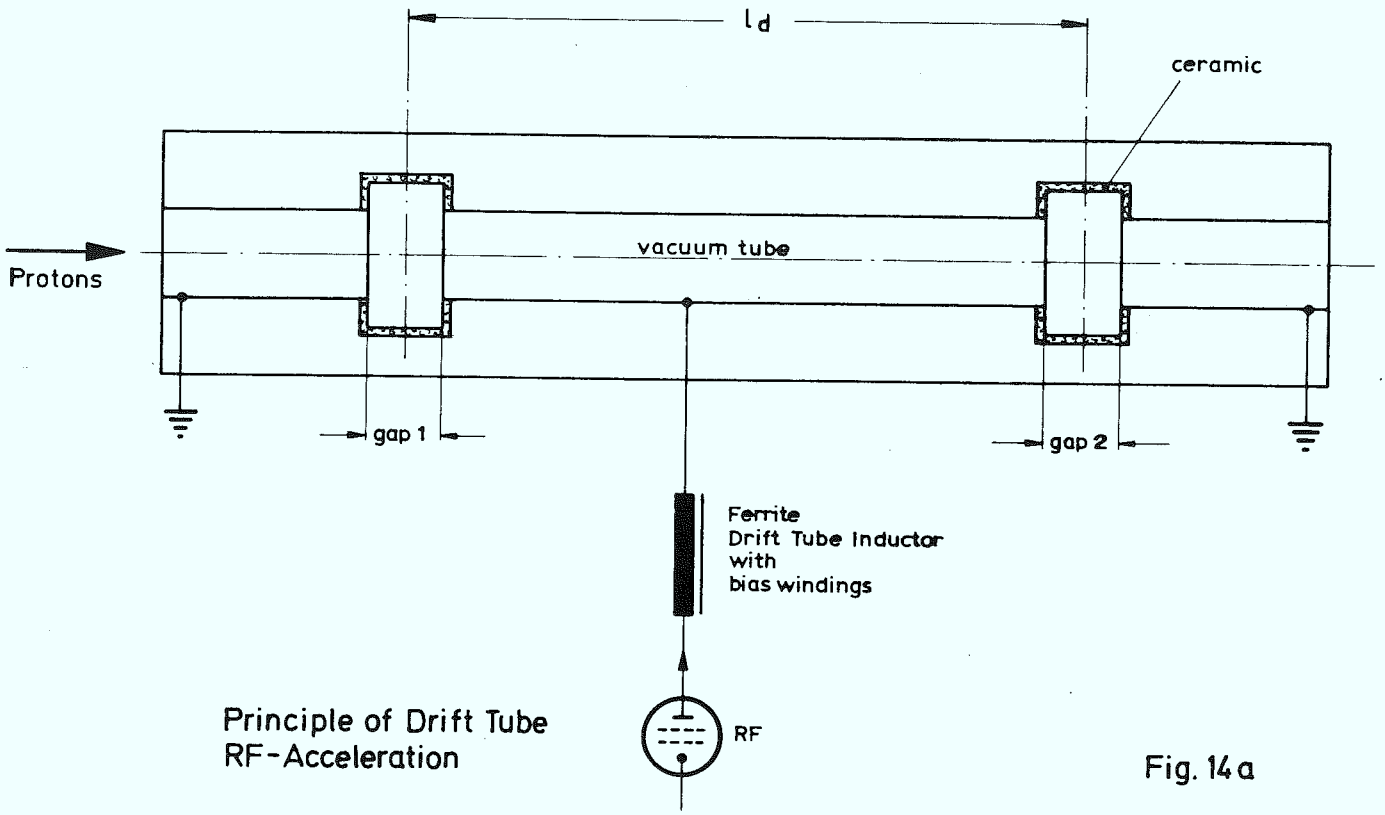

Principle of Drift Tube
RF-Acceleration

Fig. 14a

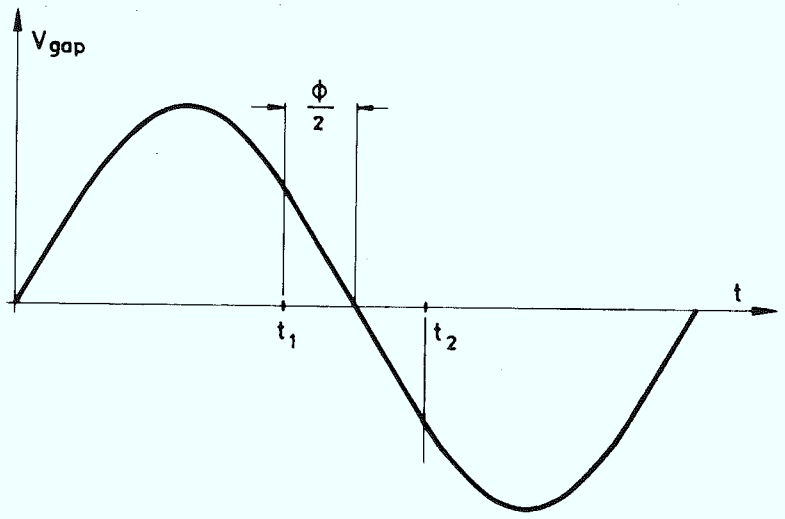

Gapvoltage versus time

Fig. 14b

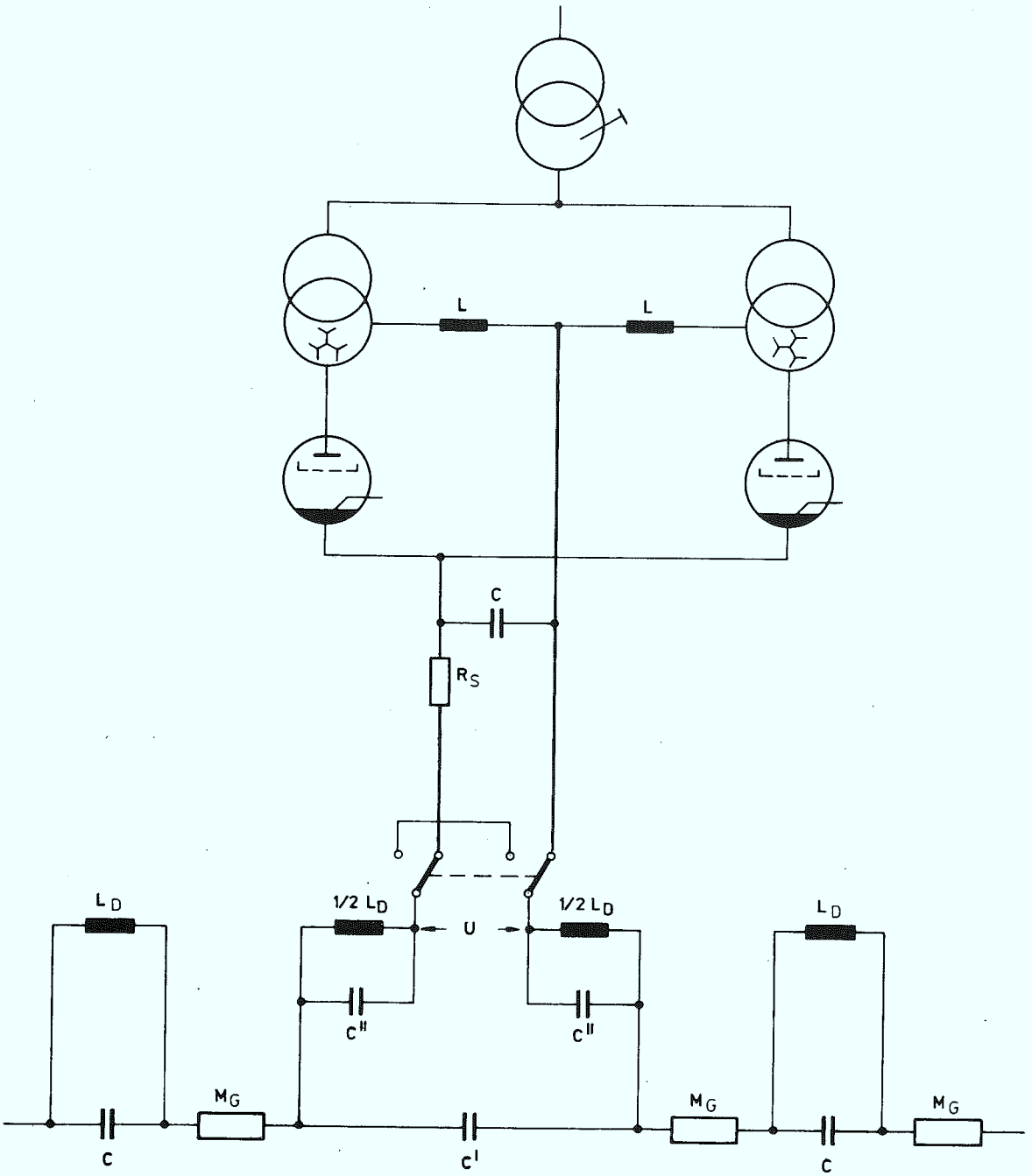

DC - Power Supply and Magnet Circuit

Fig. 15

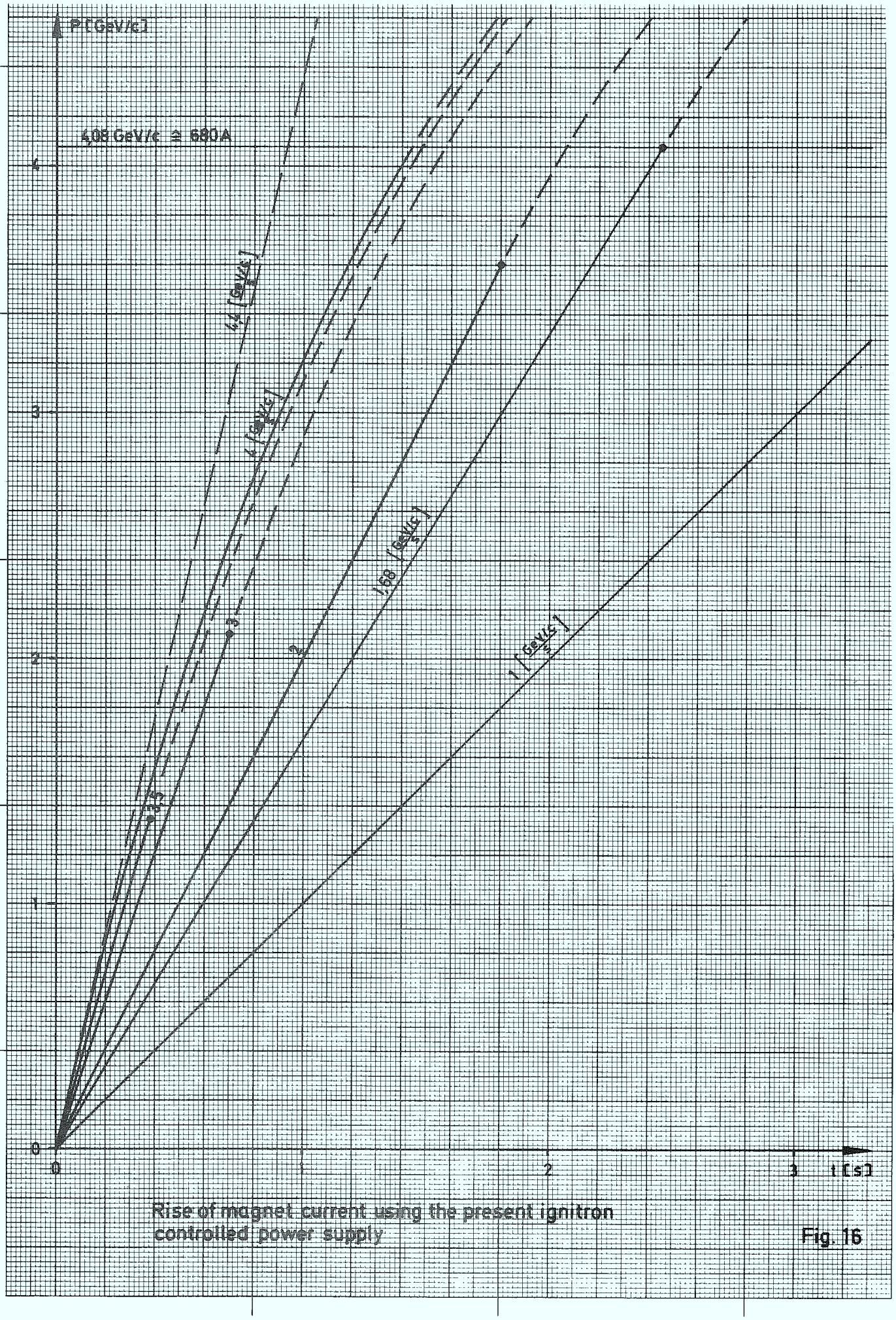

Rise of magnet current using the present ignitron controlled power supply

Fig. 16

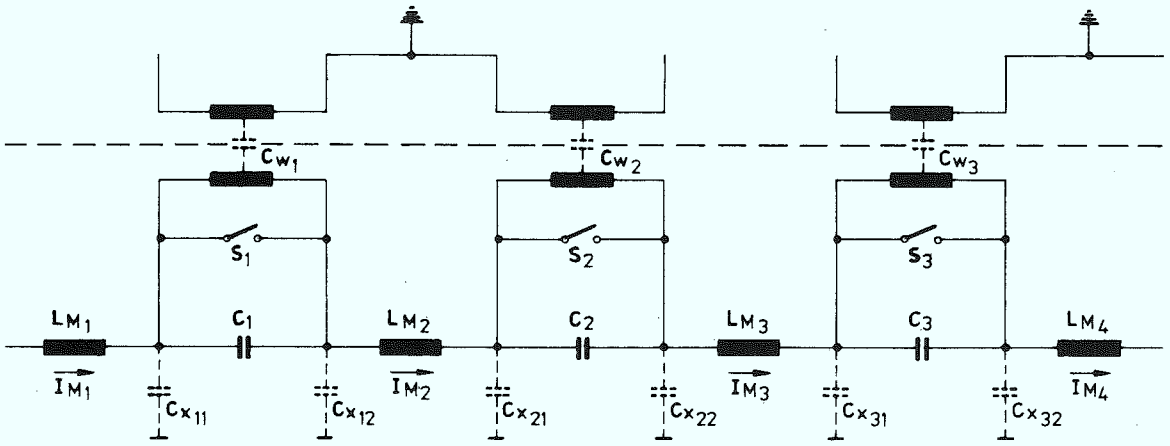

Magnet circuit with switches shorting the secondary windings of the main choke

Fig. 17 a

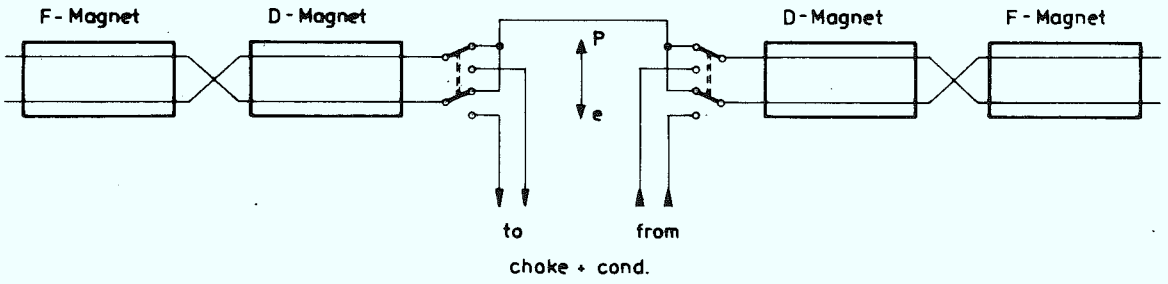

Switch circuit detail

Fig. 17 b

Fig. 17 a, b : Rearrangement of the magnet circuit for proton acceleration

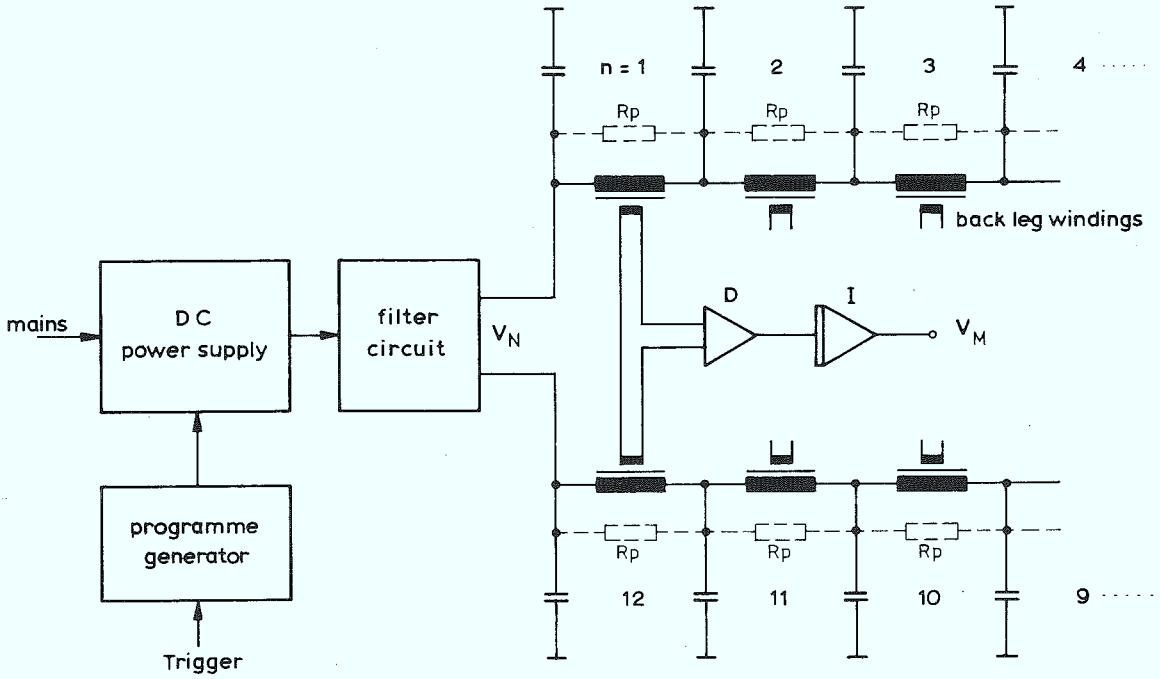

Set up for measuring the field error caused by the transient at the start of the current ramp for the synchrotron magnet Fig.18

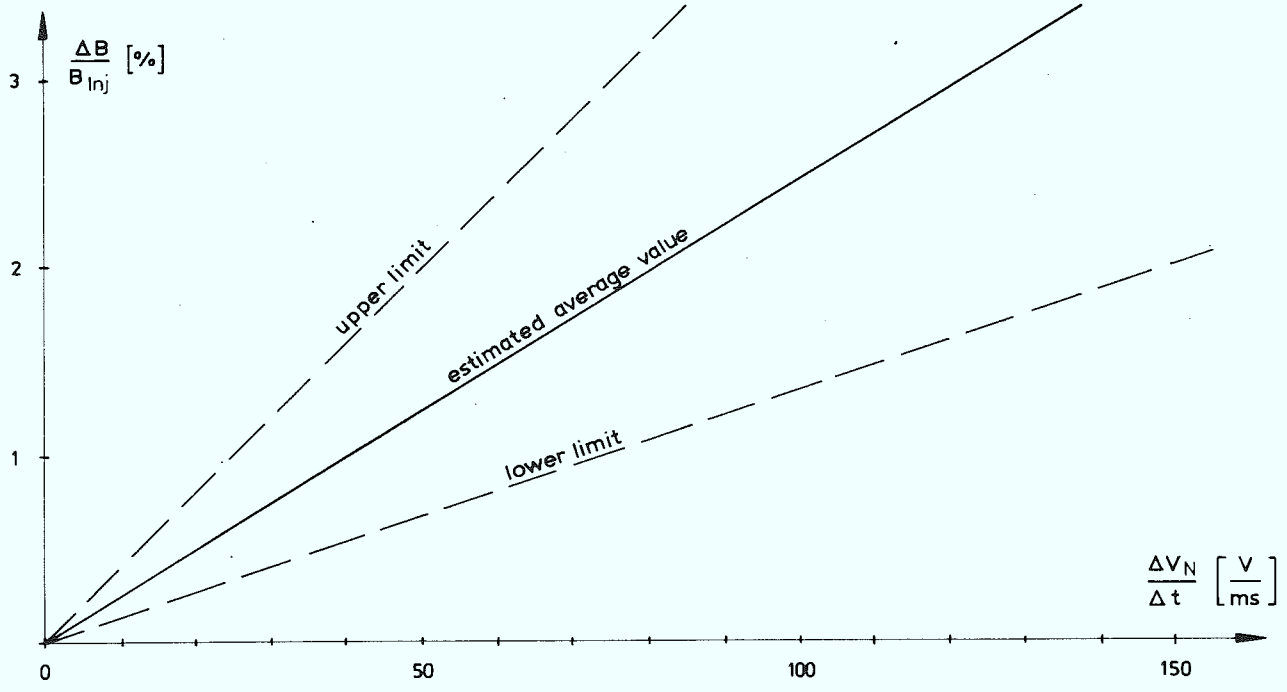

Plot of relative field errors caused by the transient of the start of "current ramp" to the synchrotron magnet Fig. 19

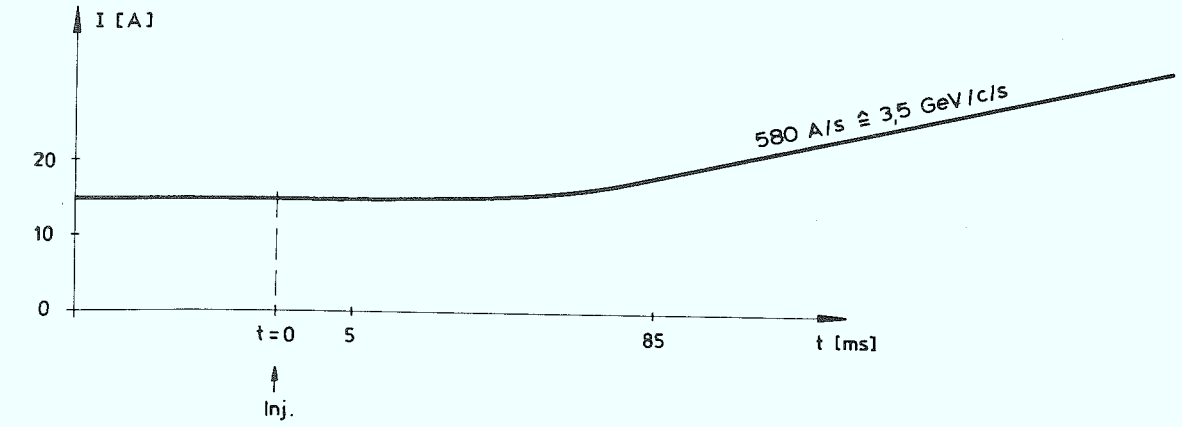

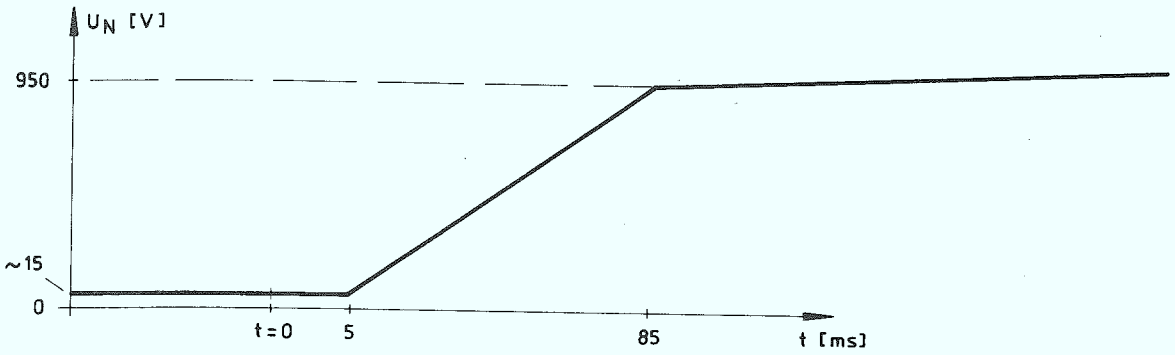

Voltage and magnet current versus time as determined by permissable closed orbit deviation of ± 5 mm

Fig. 20